Mooraj *et al. J Mater Inf* 2023;3:4
DOI: 10.20517/jmi.2022.41

Journal of Materials Informatics

Review

Open Access

A review on high-throughput development of high-entropy alloys by combinatorial methods

Shahryar Mooraj, Wen Chen*

Department of Mechanical and Industrial Engineering, University of Massachusetts Amherst, Amherst, MA 01003, USA.

***Correspondence to:** Prof. Wen Chen, Department of Mechanical and Industrial Engineering, University of Massachusetts Amherst, 160 Governors Drive, Amherst, MA 01003, USA. E-mail: wenchen@umass.edu

How to cite this article: Mooraj S, Chen W. A review on high-throughput development of high-entropy alloys by combinatorial methods. *J Mater Inf* 2023;3:4. https://dx.doi.org/10.20517/jmi.2022.41

Received: 8 Dec 2022 **First Decision:** 13 Jan 2023 **Revised:** 6 Feb 2023 **Accepted:** 7 Mar 2023 **Published:** 17 Mar 2023

Academic Editors: Tong-Yi Zhang, Xingjun Liu, Yong Yang **Copy Editor:** Ke-Cui Yang **Production Editor:** Ke-Cui Yang

Abstract

High-entropy alloys (HEAs) are an emerging class of alloys with multi-principal elements that greatly expands the compositional space for advanced alloy design. Besides chemistry, processing history can also affect the phase and microstructure formation in HEAs. The number of possible alloy compositions and processing paths gives rise to enormous material design space, which makes it challenging to explore by traditional trial-and-error approaches. This review highlights the progress in combinatorial high-throughput studies towards rapid prediction, manufacturing, and characterization of promising HEA compositions. This review begins with an introduction to HEAs and their unique properties. Then, this review describes high-throughput computational methods such as machine learning that can predict desired alloy compositions from hundreds or even thousands of candidates. The next section presents advances in combinatorial synthesis of material libraries by additive manufacturing for efficient development of high-performance HEAs at bulk scale. The final section discusses the high-throughput characterization techniques used to accelerate the material property measurements for systematic understanding of the composition-processing-structure-property relationships in combinatorial HEA libraries.

Keywords: High-entropy alloys, machine learning, combinatorial studies, high throughput, additive manufacturing, alloy design

INTRODUCTION AND MOTIVATION

Throughout history, metallurgists have altered the properties and compositions of alloys to achieve higher-performance materials. Traditional alloy design strategies involved microalloying trace elements into a primary base element, resulting in the discovery of many valuable alloys such as Cu-based bronze, Fe-based steels, and Ni-based superalloys. Over time the increasing demand for high-performance materials has led to increasingly complex alloys[1]. This trend has peaked in the past 20 years with the introduction of multi-principal element alloys or high-entropy alloys (HEAs)[2]. Unlike traditional alloys, HEAs do not contain a single primary element; instead, multiple elements in the alloy are mixed in relatively similar (almost equiatomic) concentrations. Cantor and Yeh first popularized this new alloying strategy concept in 2004 when they independently published works describing the manufacture and design philosophy of this new class of alloys[3,4]. Since the publication of these two works, the field of HEAs has exploded as such a new alloy design paradigm opens up a vast compositional space that was previously unexplored[5]. Although some fundamental questions such as phase selection and diffusion kinetics in HEAs remain elusive, many HEAs have shown high strength[6-8], large ductility[9], exceptional hardness and wear resistance[10-12], and superior corrosion resistance[13].

Despite the great potential that HEAs present for researchers, some crucial challenges must be overcome to increase their viability for future applications. While HEAs open up an uncharted multicomponent compositional space for material design, the vast compositional space makes it impractical to explore via traditional metallurgical techniques[14]. Additionally, the cost of HEAs can vary wildly due to the variety of possible elemental combinations. Some alloy systems only contain cheap transition metals (Fe, Ni, Cr)[15] that may be easy to scale, while other systems contain refractory elements (W, Nb, Ta)[16], which can significantly raise the cost of material. Finally, processing history significantly affects the microstructure and material properties even for a given nominal alloy composition. Many processing conditions including temperature, cooling rate, mechanical deformation, and irradiation can play a significant role in the formation of constituent phases and microstructures in HEAs[17-20]. Hence, processing imposes an additional and orthogonal dimension that multiplies with the huge compositional dimension and makes it more difficult to efficiently identify high-performance alloys using conventional alloy development strategies[21-23]. Thus, it is paramount for researchers to utilize efficient workflow to minimize the cost and experimental trials to study HEAs.

Over the past decade, many high-throughput material development techniques have emerged to tackle the combinatorial nature of HEAs. These techniques include magnetron sputtering, diffusion multiples, and additive manufacturing. Magnetron sputtering uses a magnetically confined plasma to accelerate positively charged ions toward a target material, leading to the sputtering of the target atoms onto a substrate to form a thin film with a thickness ranging from a few nanometers to a few microns[24]. A combinatorial materials library can be built by sputtering multiple elemental targets onto a single substrate[24-29]. The diffusion multiples method involves arranging different metals such that they are physically touching. Then this configuration is heated to an elevated temperature that enables atomic diffusion across the interfaces between the different metals. This process leads to a compositional gradient near the interface that serves as a compositional library[30-34]. Despite the large compositional space that diffusion multiples and magnetron sputtering can achieve, these approaches encounter some difficult issues. Both techniques involve samples of microscopic length scales, and thus, the microstructures and material properties observed from these libraries may not be representative of these materials at bulk scales. In addition, magnetron sputtering involves extremely high cooling rates on the order of 10^{10} K/s, which are substantially higher than those involved in routine metal manufacturing[35,36]. As such, the phases and microstructures in sputtered thin films are almost exclusively polymorphic or even amorphous and thus do not represent the microstructures of bulk materials for most practical applications.

Additive manufacturing (AM), also called 3D printing, is a technology to make objects from 3D digital data, usually layer upon layer, as opposed to subtractive manufacturing technologies[37]. There exist several types of AM systems that can be used to produce metal alloys: powder bed systems, powder feed systems, thermal spray systems, and wire feed systems. In the case of a powder bed system, the feedstock powders are spread over a flatbed, and a 2D pattern is selectively melted over the bed using either a laser or electron beam as a heat source[38,39]. Powder feed systems flow powders through a delivery nozzle using a carrier gas and then melt the powders onto the substrate as it impacts the substrate using heat from a laser[40,41]. Thermal spray 3D printing (TS3DP) systems spray heated powders at high velocities onto a substrate leading to bonding between powder particles as they impact the substrate surface. This allows parts to be built layer by layer without the large heating and cooling rates of laser-based techniques[42]. Finally, wire feed systems use metal wires as feedstock and can use either electric- or plasma-based welding arcs to melt the wire and build a part layer by layer[43-46]. AM of multiple elemental feedstock powders or wires offers the capability to build large compositional libraries at bulk length scales. Furthermore, careful control of the printing parameters during AM, such as laser power and scan speed, allows for tailoring the cooling rates and resulting solidification microstructures to expand the material development space.

In order to rapidly discover new HEAs with desirable properties, researchers need to utilize an efficient workflow to leverage the strengths of various design and characterization techniques. Figure 1 illustrates a typical protocol for high-throughput development of HEAs. First, the elements of interest are selected based on their fundamental properties and interactions, which are fed into a high-throughput computational method like machine learning, molecular dynamics, CALculation of PHAse Diagram (CALPHAD), or first-principles calculations. These computational methods can then predict the bulk materials' phase formation, microstructure, and properties for initial screening of potential compositions of interest. Subsequently, high-throughput manufacturing can be used to fabricate the vast material library and high-throughput materials characterization enables rapid measurements of the material properties. This review focuses on high-throughput computational techniques, synthesis methods, and characterization studies that produce and analyze alloys with reasonable cooling rates at *bulk* scale. First, this review explores the high-throughput computational methods that can easily identify the potential compositions that show promising properties for structural or functional applications. Then, it discusses the high-throughput manufacturing of bulk compositional libraries encompassing a wide range of potentially interesting alloys by AM. The final section of this review describes some high-throughput characterization techniques to accelerate screening of multicomponent metal alloys. This combination of high-throughput methods offers a guideline for researchers to discover new alloys rapidly and efficiently.

OVERVIEW OF HEAS

Definition of HEAs

There currently exist two well-accepted definitions of HEAs. The first one, referred to as the "compositional definition", states that HEAs are alloys with multiple principal elements (at least 5) where each principal element makes up 5 at. % to 35 at. % of the overall composition[4,48]. The most commonly studied HEA is the Cantor alloy system which contains equiatomic CoCrFeNiMn, a prime example of this definition[2,3]. Figure 2A illustrates this high-entropy region within a ternary phase diagram, with the center of the phase diagram covered by the high-entropy region[49]. It should be noted that the edges of the phase diagram in Figure 2A may contain two or more elements to match the composition definition. Additionally, minor elements can be added to a base HEA system to tune its properties further[50].

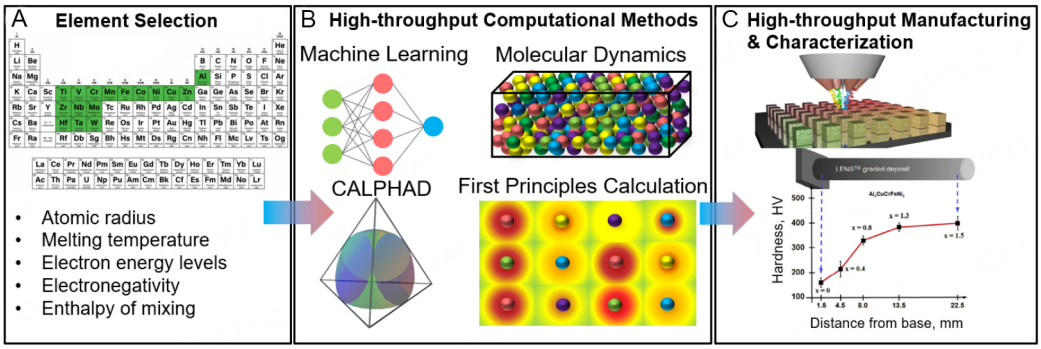

Figure 1. Schematic illustration of a typical protocol for high-throughput development of HEAs. (A) Selection of elements for a prospective alloy system; (B) high-throughput computational methods are used to select a range of promising compositions that can be explored experimentally; (C) high-throughput manufacturing and characterization of the promising compositions selected via computation to determine the target composition. The lower illustration in (C) is quoted with permission from Borkar *et al.*[47], copyright 2016, Elsevier. HEA: high-entropy alloy.

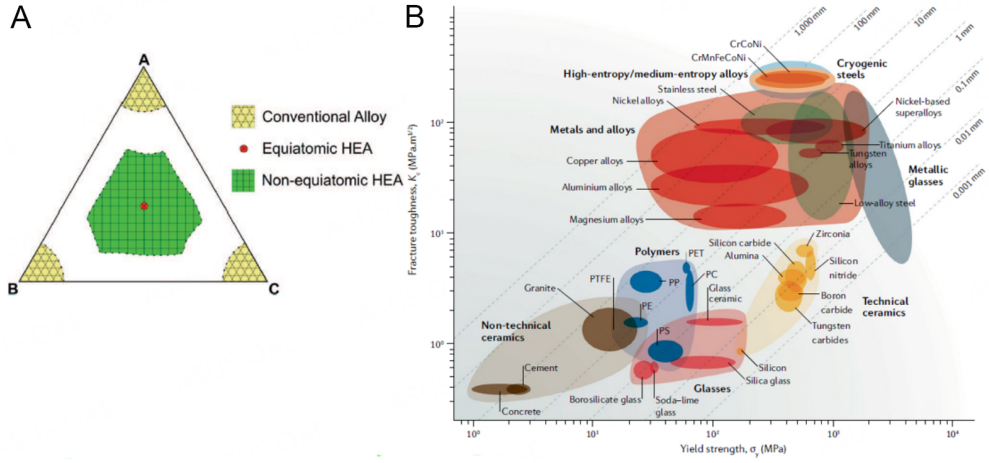

Figure 2. (A) Schematic illustration of the composition space of conventional alloys, equiatomic HEAs, and non-equiatomic HEAs. This figure is quoted with permission from Li *et al.*[49]; (B) ashby chart of the yield strength *vs.* fracture toughness of many material groups showing high/medium entropy alloys have excellent damage tolerance, adapted from George *et al.*[5], copyright 2019, Springer Nature. HEA: High-entropy alloy.

The second widely accepted definition is based on the mixing entropy of an alloy system, assuming an ideal random solution state. The mixing entropy is calculated as $\Delta S_{mix} = -R * \sum_{i=1}^{n} x_i \, ln(x_i)$ where R is the ideal gas constant, n is the number of principal elements, and x_i is the atomic fraction of the ith element[48]. Yeh *et al.* separated the alloy design space into three regimes where a low entropy alloy has $\Delta S_{mix} < 0.69R$, a medium entropy alloy has $0.69R < \Delta S_{mix} < 1.61R$ and a HEA has $1.61R < \Delta S_{mix}$[51]. It should be noted that the definition of mixing entropy above includes the assumption that the random solution state is defined as the liquid state or a high-temperature solid solution state such that the atoms have enough energy to maintain completely random configurations[51]. However, it has been pointed out by Miracle *et al.* that the above threshold for HEAs would exclude certain non-equiatomic alloys with five principal elements, as calculations show that such alloys exhibit $\Delta S_{mix} < 1.61R$[48]. Miracle *et al.* also pointed out that others have suggested using a threshold of $1.36R < \Delta S_{mix}$ which would include the alloys that were excluded by the threshold proposed by Yeh *et al.*, making the entropy definition more consistent with the principal element definition[48].

Four core effects

Despite their relatively short history, HEAs have already shown great potential for practical applications. Their properties are already competitive with and even exceed those of state-of-the-art materials. This potential is highlighted in Figure 2B, which illustrates the exceptional combination of high toughness and yield strength of HEAs compared to traditional structural materials[5]. The origin of these outstanding properties is often attributed to four core effects associated with HEAs: the high entropy effect, severe lattice distortion, sluggish diffusion, and cocktail effect[48]. Figure 3 presents a schematic illustration of the four core effects associated with HEAs. Each of these effects contributes to the unique properties observed in HEAs, and these contributions will be discussed below.

High entropy effect

Traditional alloying strategies suggest that alloys with multi-principal elements form multi-phase, brittle intermetallic systems[51]. However, many works on HEAs show they could achieve metastable and stable single-phase solid solutions[53-55]. Even in HEAs that show multiple phases, the number of phases is much lower than the maximum number predicted by the Gibbs phase rule[56-58]. These results suggest that the high mixing entropy leads to increased mutual solubility of elements in HEA systems. The effect of high mixing entropy is described by the equation for Gibbs free energy of formation, which implies that phases with high entropy will have a lower Gibbs free energy and thus be more stable[59]. Thus, the high mixing entropy aids in stabilizing single-phase solid solutions as long as this contribution overcomes the enthalpy of formation of possible intermetallic phases, especially at elevated temperatures. Additionally, this relationship also implies that the contribution of the mixing entropy to the Gibbs free energy decreases at lower temperatures and suggests that HEAs in the form of solid solutions at high temperatures may become metastable and decompose at low temperatures. For example, Stepanov *et al.* showed that Cantor alloy exhibits a typical single-phase face-centered cubic (FCC) structure upon quenching; however, it can decompose with the precipitation of a secondary Cr-rich σ-phase after prolonged annealing at 600 °C[60]. This representative finding again underscores the importance of processing history in the phase selection of HEAs, which will be discussed in later sections.

Sever lattice distortion

In HEA systems, various atoms with different atomic sizes lead to varying bond configurations and local lattice energies. These bond configurations create a high lattice distortion within the crystal structure[61,62]. The severe lattice distortion has been experimentally confirmed in many HEA systems via X-ray diffraction (XRD), neutron diffraction, and TEM[62-66]. Such severe lattice distortion leads to more diffuse scattering through the lattice and causes the broadening of diffraction peaks with a decrease in the peak intensities compared to traditional dilute alloy systems. The increase in lattice distortion also impedes the motion of dislocations through the matrix, which leads to solid solution strengthening. Traditional solid solution strengthening models typically involve the contributions of solute atoms to a matrix of solvent atoms. Still, these models are challenging to apply to HEAs as the solvent and solute atoms cannot be clearly distinguished[59]. To that end, new solid solution hardening models have been developed by accounting for the lattice and shear modulus distortion in the local environment near each constituent atom[61,67]. The lattice distortion within HEA systems has also been shown to correlate strongly with the stability of various phases. For example, single-phase solid solutions tend to be more stable in systems with low lattice distortions. In contrast, intermetallic and multi-phase structures are more likely to form in systems with high lattice distortions. This effect can sometimes outweigh the effect of high configurational entropy in phase selection[55,68,69].

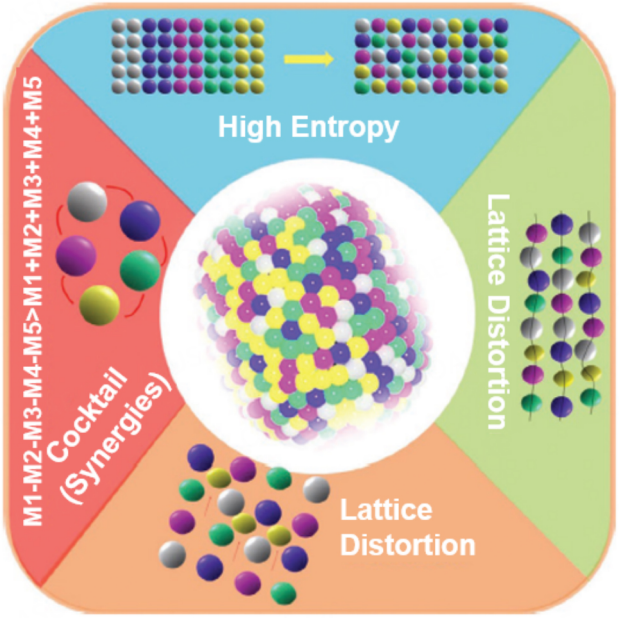

Figure 3. Schematic illustration of properties of HEAs. This figure is quoted with permission from Li *et al.*[52], copyright 2021, John Wiley and Sons. HEA: High-entropy alloy.

Sluggish diffusion

Diffusion through HEAs can be much slower than diffusion in conventional alloys. Many researchers have investigated the elemental diffusion in HEA systems and have found that the diffusivities are often much lower than those in binary or dilute alloy systems[70-72]. This sluggish diffusion can improve the stability of solid solution phases as harmful intermetallic phases can be largely suppressed. Intermetallic phases can only form under non-polymorphic solidification conditions, which require long-range diffusion. Additionally, metastable solid solutions form under polymorphic crystallization conditions, which only require topological atomic rearrangements on the atomic length scale[23]. Thus, the sluggish diffusion in HEAs suppresses the long-range diffusion that would lead to the formation of brittle intermetallic phases and instead promotes polymorphic crystallization to form solid solutions. Additionally, the coarsening of grains can be inhibited due to sluggish diffusion, leading to improved thermal stability and thermomechanical performance at elevated temperatures[73-75].

Cocktail effect

Dr. Ranganathan first proposed the cocktail effect to describe the synergistic nature of compositionally complex alloys[76]. This effect describes the unexpected properties observed in HEAs, bulk metallic glasses, and super-elastic and super-plastic metals (also called "gum" metals)[48]. Unlike the other effects described earlier, the cocktail effect does not predict the expected properties of HEAs. Still, it serves as a reminder that certain elemental combinations can achieve synergistic effects that are not predicted from the base constituent elements.

HIGH-THROUGHPUT COMPUTATIONAL METHODS TO DESIGN HEAS

As previously mentioned, the compositional space opened by the concept of HEAs is vast. This design space is too large to explore through traditional trial-and-error means. Thus, it is of significant interest to identify promising compositions and phases via high-throughput computational methods[77]. These computational methods include machine learning, first-principles calculations, molecular dynamics, and CALPHAD. The

field of high-throughput computational studies is extremely wide and covers too many topics to discuss succinctly. As such, the discussion of computational methods is limited to studies focused on phase formation and mechanical properties of HEAs to illustrate the potential advantages and disadvantages of the previously mentioned methods.

Machine learning

Machine learning (ML) is a powerful computational tool to rapidly explore vast design space through statistical methods[78]. These methods include artificial neural networks (ANN), support vector machines (SVM), and decision trees, which can often be used to quantitatively predict material properties such as hardness[79] or to predict qualitative factors such as the expected phases of a given alloy composition[80]. Over the past decade, as computational power has continued to increase, there has been an explosion in the topics of machine learning and big data[81]. Machine learning methods have an extremely high potential to handle large databases due to their statistical nature. This section includes examples from literature of various ML techniques and methods that are representative of the state-of-the-art results achieved in the field.

ML techniques are capable of predicting the structure and properties of various alloys in reasonably short periods. However, this predictive capability is largely dependent on the size and quality of the training data, a thorough consideration of appropriate input variables (also known as feature engineering), and the choice of ML model[82]. Typically robust databases of training data only exist for materials that have been well studied, such as the Ni-Ti-Hf shape memory alloy (SMA) systems[83]. For example, Liu *et al.* developed Gaussian process regression (GPR) models to estimate thermal parameters related to the martensite and austenite finish temperatures in a Ni-Ti-Hf alloy system to design a SMA[83]. The predicted parameters were described as $\bar{T} = (A_f + M_f)/2$, and $\Delta T = A_f - M_f$, where A_f and M_f are the austenite finish and martensite finish temperatures, respectively. The value of $\bar{T}$ represents the average of the austenite finish and martensite finish temperatures and thus illustrates the temperature region where an SMA is expected to transform. Tuning this range can be useful in aerospace applications where autonomous actuation can be induced due to the temperature difference of the surroundings at take-off (typically 275 K) and cruising (usually 215 K)[83]. On the other hand, ΔT represents the total temperature range of the austenite finish and martensite finish temperatures, indicating the hysteresis during the transformation. A low ΔT can lead to more efficient actuation when the martensitic and austenitic phase transformations are activated.

As previously mentioned, an essential aspect of building an ML model is the determination of the input variables that will most accurately predict the output variables. Typically, adding more input variables can improve the model's accuracy, as variables that do not correlate strongly with the output variables will have to be emphasized less through training sets. However, using too many input variables increases the dimensionality of the model, making it computationally expensive to execute. Additionally, the solution space formed by many input variables can often contain local minima that require many iterations to escape. For this reason, Liu *et al.* initially started with 48 input variables based on the relevance of those variables to the physical processes involved in martensitic and austenitic phase transformations[83]. These chosen features included fundamental atomic properties (e.g., atomic radius, atomic number, relative atomic mass, etc.), thermal properties (e.g., melting point, boiling point, the heat of fusion, thermal conductivity, etc.), overall alloy compositions, electronic configurations, and process conditions (e.g., solution temperature, aging temperature, etc.). This variable space was refined via mutual information (MI) and Pearson correlation (PC). MI indicates the dependency of the output variable on the input variables, which ensures that only the most impactful variables are used. In contrast, the PC between the two variables illustrates their correlations. Input variables strongly correlated to each other produce redundant

information and can thus be disregarded. Using this method, Liu *et al.* built a model that explored a 4500-point compositional space in which seven compositions were identified that exhibit $230 < \bar{T} < 260$ and the lowest ΔT values. These results illustrate ML models' capabilities to selectively tune a material system's properties using robust training datasets from previous studies and carefully selected input variables.

Most ML techniques are black-box ML with limited interpretability, which can hinder the development of chemical insight into the origin of preferable properties. Recently, a new method to implement ML described as a ML-based alloy design system (MADS) has been developed to predict alloys and maximize the hardness within an Al-Co-Cr-Cu-Fe-Ni-V alloy system[79]. This method is schematically illustrated in Figure 4A and consists of four steps. First, a database containing alloy compositions within the selected system and their measured hardness is established. Then a set of 142 features to model the hardness is established and refined to remove all except the five most crucial factors. This refinement step is important to reduce the computational cost and redundancy of information within the ML model. A model utilizing the most critical parameters is constructed and then executed to optimize the composition toward maximum hardness. Finally, the designed alloy compositions are experimentally fabricated and tested to verify the predicted properties. The five features selected were the average deviation of the atomic weight, the average deviation of the period column in the periodic table, the average deviation of the specific volume, the valance electron concentration, and the mean melting point for the alloy. After exploring the presented alloy system, the optimized composition was determined to be $Co_{18}Cr_7Fe_{35}Ni_5V_{35}$ which was predicted to have a hardness of 1,002 HV and was experimentally verified to show a hardness of 1,148 HV, showing the prediction is in good agreement with the experimental value. This new HEA exhibits about 25% greater hardness than the maximum hardness in the original training dataset. The hardness improvement illustrates ML methods' ability to take previous experimental data and extrapolate it to discover new compositions with better properties than previously achieved.

Artificial neural networks (ANNs) are common ML methods that use a layered architecture of input, hidden, and output nodes trained to predict useful material properties such as phase formation, hardness, and yield strength. The input layer consists of multiple nodes which hold values of the parameters that are known either a priori or from databases. Then each node in the 1st hidden layer is calculated by a weighted sum of the nodes from the input layer. Nodes in subsequent hidden layers are calculated by a weighted sum of the nodes from the previous layer. Finally, the output layer consists of the target/output parameters calculated from a weighted sum of the nodes from the hidden layer immediately preceding the output layer. These parameters can include the predicted properties of the studied alloys, such as the hardness of a material, the elastic properties, phase prediction classifier etc. The weights for every calculated sum are initialized as a best guess and then adjusted to minimize the error between the predicted and experimental values for training data. Once the error is minimized, the adjusted weights can then be used in conjunction with input data for new alloy systems outside of the training set to predict properties of interest[81,84,85].

Notably, Nassar *et al.* used two different ANNs (NN1 and NN2) to predict the phase formation with 37 possible elements in the alloy composition[86]. NN1 had only composition data as its inputs and, thus, only 37 input nodes. NN2 used composition data and some calculated thermodynamic properties of each composition, such as the entropy of mixing, enthalpy of mixing, valence electron concentration (VEC), atomic radius difference, and Pauling electronegativity difference. The output node values were a binary of 0 or 1, where 1 indicates the formation of a single-phase solid solution (SS) or a solid solution plus intermetallic (SS + IM). At the same time, 0 predicts a primary IM phase or IM + amorphous phase structure. After training, the neural networks could accurately predict the type of microstructure given an arbitrary composition with 92% and 90% accuracy for NN1 and NN2, respectively. The improved accuracy

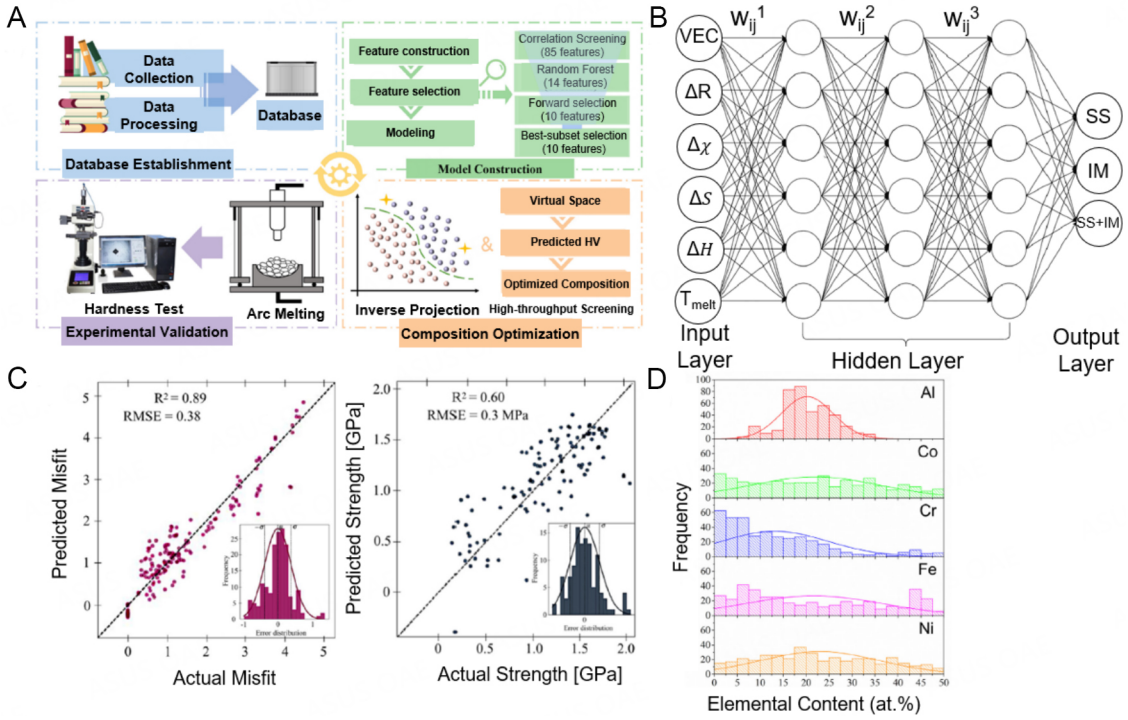

Figure 4. (A) Schematic diagram of machine learning-based approach to design new HEAs. This figure is quoted with permission from Yang *et al.*[79], copyright 2022, Elsevier; (B) schematic illustration of artificial neural network method, adapted from Risal *et al.*[87], copyright 2021, Elsevier; (C) actual versus predicted misfit and yield strength for 10-fold cross-validation of machine learning models, insets show the error distribution around the mean. This figure is quoted with permission from Vazquez[90], copyright 2022, Elsevier; (D) elemental content distribution of predicted eutectic HEAs, adapted from Wu *et al.*[6], copyright 2020, Elsevier. HEA: High-entropy alloy.

of NN1 is surprising, given that it only used the elemental composition as input, while NN2 included features related to thermodynamic properties.

Another work that shows consistent results with NN2 is that of Risal *et al.*, where 598 alloy compositions extracted from the literature were used as the training set, and the input parameters included the VEC, melting temperature of the alloy, enthalpy of fusion and variance of atomic radius[87]. The basic structure of the neural network used in their work is illustrated in Figure 4B. Interestingly, they achieved a prediction accuracy of 90.66%, slightly lower than that of NN1 and almost the same as NN2 in Nassar *et al.*'s work[86]. This result can be rationalized by the fact that NN typically only elucidates the correlation between parameters and thus may not always reveal the underlying physical connection between the input and output variables. Many examples exist in the literature on NNs, providing valuable predictions for HEAs' microstructure type and material properties. However, further study is needed to understand the mechanisms that lead to these valuable properties.

A common criticism of ML models is that they often lack interpretability despite their high predictive accuracy[88,89]. Sure-independence screening and sparsifying operator (SISSO) is an example of an ML method that can produce easy-to-understand relationships between the input and output variables. SISSO can output these relationships as analytical equations such that the dependence of the output variables on each input variable can be easily understood. Vazquez *et al.* recently used SISSO to predict the mechanical properties of alloys within a Ta-W-Nb-Mo-V refractory HEA (RHEA) system[90]. This method functions very differently from other ML algorithms as most methods attempt to filter the possible valuable features to

build an input space that is computationally efficient to analyze, as shown in previous examples. In the case of SISSO, the features are compiled as mathematical functions (descriptors) by applying mathematical operators to arbitrary groupings of the features. The descriptor space is then narrowed using sure independence screening (SIS) to identify descriptors that most strongly correlate to the target properties. Then, the sparsifying operator (SO) produces a linear model of the descriptors that best predicts the target property[91]. In this way, SISSO can produce models which converge even if the initial feature space is larger than the data set. Additionally, Vazquez *et al.* point out that SISSO is computationally inexpensive compared to typical ab-initio calculation methods like DFT[90]. Figure 4C shows the prediction of misfit volume and yield strength *vs.* the actual values calculated by DFT. The accuracy of the prediction of the misfit volume suggests that SISSO can reliably predict the mechanical properties of RHEA systems while remaining computationally much cheaper than DFT calculations. While the yield strength prediction overall shows a very low root mean squared error (RMSE), the R2 value is quite large, which arises due to limited experimental data and a lack of documentation of the processing conditions related to many compositions in the yield strength database. This result highlights the need for larger, more robust, and more detailed databases of experimental HEA data to improve the training quality of future ML models.

As previously mentioned, ML models can predict phase formation using solely composition information. This concept is taken even further by Wu *et al.*, who used a NN to study the effect of each element in a HEA system on the phase to predict the primary phase fraction after casting[6]. With this technique, they could design near-eutectic compositions within the Al-Co-Cr-Fe-Ni system[6]. The database[6] to train the model was prepared using experimental data from the literature, and CALPHAD calculations were performed using the nickel-based superalloy database TTNI8. Wu *et al.* chose to only use the elemental compositions as the input nodes and the primary phase fraction as the output node. The primary phase fraction was defined as 0 for eutectic compositions. In contrast, hyper- and hypo-eutectic compositions showed a positive value when FCC was predicted as the primary phase and a negative value when body-centered cubic (BCC) was predicted as the primary. After training and executing the NN, the authors identified 400 near-eutectic compositions and correlated them with the atomic fraction of each element. This plot is shown in Figure 4D, where it can be seen that the majority of the near-eutectic compositions fall into the region when Al content (at. %) is between 15% and 20% and the Cr content is below 25%. The other elements do not seem to significantly affect the formation of eutectic structures, which suggests that the Al and Cr contents are most crucial for eutectic structure formation in this alloy system. Thus, the NN was first used to predict the amount of Al that needed to be added to an equiatomic CoFeNi alloy to form a eutectic microstructure and how much Cr could be added to maintain that microstructure. Finally, the ratios of the other elements were further adjusted to predict a near-eutectic microstructure. The best composition based on the criteria of stable eutectic microstructure was $Ni_{32}Co_{30}Fe_{10}Cr_{10}Al_{18}$. This work presents the potential of ML models to refine a huge design space containing thousands of unique compositions down to a single optimized composition that can then be experimentally studied in detail.

While ML techniques such as those discussed in this section can readily analyze extremely large data sets, their accuracy depends heavily on the robustness and comprehensive nature of experimentally verified training sets[77]. There is currently a severe lack of such high-fidelity datasets to accurately train ML models to ensure ML can accurately predict the properties of future alloy systems[92]. In the meantime, as these databases expand, the scientific community is also implementing other computational methods that do not rely so heavily on previous results to predict future alloying behavior. These methods include first-principles calculations, molecular dynamics (MD), and CALPHAD calculations and will be discussed in the following sections.

First-principles calculations

First-principles calculations (also called ab-initio) are computational methods that rely purely on fundamental quantum physical laws without additional assumptions[93]. The literature on first-principles methods is vast and presents a comprehensive overview beyond the scope of this work. This section will provide a sufficiently broad outline of the general concepts, advantages and disadvantages of these techniques pertinent to combinatorial studies of HEAs[93]. The main strength of these methods is that they do not require previous empirical observations of the predicted properties, and thus very little prior work is needed to implement them[94]. The most common practical implementation of ab-initio calculations is density functional theory (DFT) in the Khon-Sham formalism[94,95]. This method maps the quantum-mechanical many-electron Schrodinger equation onto an effective one-electron problem using electron density as a key variable. This mapping also requires the use of the exchange-correlation functional of the electron density which is not known for most systems and must be approximated either with the local density approximation (LDA)[96,97] or the generalized gradient approximation (GGA)[98-100]. Once these fundamental functions are calculated, the overall energy of the system can be calculated and used to determine the energy of formation for the possible phases of the system. This result can help researchers determine the stability of different phases to determine which phases are likely to form. It should be noted that in its initial state, DFT is a ground state theory and thus only provides the ground state energy at 0 K for a given configuration of atoms[94]. These results can be combined with thermodynamic concepts and statistical sampling techniques to bridge the gap between 0 K to a finite temperature[94].

Despite the strong predictive power of ab-initio calculations, they often suffer from high computational costs, which can significantly decrease the ability of researchers to explore the vast design space that is necessary to build accurate property maps for HEAs. To overcome this challenge, many researchers either combine first-principle calculations with more high-throughput methods like ML[101] or use new algorithms and models to improve the computational efficiency to the point where first-principles calculations can be used to explore hundreds to thousands of compositions in relatively short periods. Examples of such works will be discussed in this section.

One approach that is considered highly promising toward high fidelity and high throughput computations of HEAs is based on the small set of ordered structures (SSOS) containing several atoms[92]. This method works well to predict properties of equiatomic configurations of HEAs but loses computational efficiency when employed for non-equiatomic compositions. Sorkin *et al.* implemented a preselected set of small ordered structures (PSSOS) approach to address the issue of computational efficiency and used it to estimate the stability of BCC and FCC phases within the Al-Co-Cr-Fe-Ni system[92]. Traditionally the SSOS method uses a set of small, ordered structures (SOS) to model a HEA with a given composition. First, symmetry-unique SOS are constructed using non-conventional, non-primitive unit cells of cubic lattices. Each SOS has a unique pair correlation function. The complete set of possible SOS solutions is constructed and optimized using DFT. Then a small subset of SOS is selected by matching the pair correlation function of the target composition as a linear combination of the pair correlation functions of the selected SOS. This small set of SOS constitutes the solution of the SSOS. Screening the entire SOS solution space is impractical when studying HEAs, so the authors restricted their SOS space to those containing 5, 6, or 7 atoms. They selected the most frequent SOS structures in the solution set to further reduce the SOS space and only optimized those using DFT. This selection decreases the original SOS from over 50,000 sets to 1,500.

Through the above-mentioned process, the authors can predict the formation energy and density of the alloy system's BCC and FCC phases of 8,801 compositions. This result is exemplified in Figure 5A, which shows a plot of the formation energy and density of the BCC phase with varying Al and Cr compositions. Here the marker color represents the Ni content, and the marker size represents the Co content. It can be

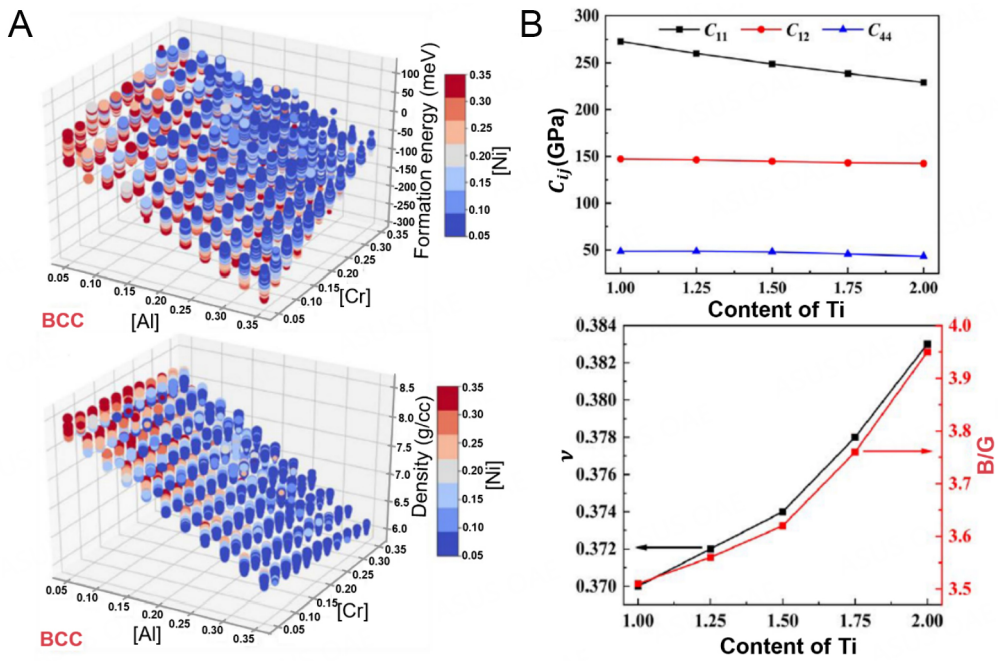

Figure 5. (A) Predicted formation energy and density per atom of BCC lattice structure in AlCoCrFeNi system calculated via the SSOS method as a function of Al and Cr content, the color denotes the Ni content, and marker size denotes the Co content. This figure is quoted with permission from Sorkin *et al.*[92]; (B) plot of predicted elastic constants (C_{11}, C_{12}, C_{44}), Poisson ratio, and Bulk modulus to shear modulus ratio calculated with the VCA model as a function of Ti in the Ti_xVNbMo system. This figure is quotedwith permission from Chen[104]. BCC: Body-centered cubic; SSOS: small set of ordered structures.

seen that the addition of Al leads to a substantial decrease in the formation energy of the BCC phase. After calculating the same parameters for the FCC phase, the authors found that the difference in the formation energies of BCC and FCC ($\Delta E_{BCC \rightarrow FCC} = E_{BCC} - E_{FCC}$) goes from positive to negative as the Al content increases, which is consistent with DFT calculations of the system. These results illustrate that the PSSOS method provides a new opportunity to achieve similar accuracy predictions of phase formations as DFT but with much cheaper computational costs, making this method highly suitable for high-throughput exploration of HEA space.

Virtual crystal approximation (VCA) serves as a computationally efficient alternative to more complex first-principles methods like special quasirandom structure (SQS) and similar local atomic environment (SLAE). Normally, DFT methods must use approximations to study highly disordered systems[102]. The approximation is carried out by constructing a supercell that contains multiple disordered configurations with artificially imposed boundary conditions[102]. However, such calculations require large supercells that are computationally taxing to utilize in DFT calculations. VCA deals with this issue using a pseudo-potential that averages the properties of each atom in different positions in the lattice cell. Ramer and Rappe previously investigated multiple methods to produce the averaged pseudo-potential such as averaging the pseudo-potentials for each atom within the lattice and averaging 'all-electron results'[103]. It was found that the averaging of 'all-electron results' provided the most accurate result when compared to experiments. This method involved averaging the Coulombic potentials and charge densities of the constituent atoms and then using these values to generate wavefunctions that are self-consistent solutions to the Kohn-Sham equation[103].

The computational efficiency of VCA makes it uniquely suited to explore HEA systems, as shown by Chen *et al.*, who used the VCA method to explore the effect of Ti within the Ti_xVNbMo system[104]. VCA only requires the construction and analysis of a primitive cell, while other DFT methods require the use of a supercell as previously discussed, making them much more difficult to calculate. Since VCA has previously achieved reliable results for studying RHEA systems, Chen *et al.* proposed that it is reasonable to implement it to analyze the mechanical properties of this RHEA. Figure 5B illustrates the effect of Ti content on the lattice elastic constants and elastic properties [Poisson ratio and ratio of the bulk modulus to the shear modulus (B/G)]. Looking at the lattice elastic constants, it is clear that $C_{12} > C_{44}$ for all compositions, and the Cauchy pressure ($C_p = C_{12} - C_{44}$) is positive for all the compositions. This suggests that the nature of the bonding for all these compositions remains metallic. The Born-Huang mechanical stability criterion is also met ($C_{11} - C_{12} > 0$, $C_{11} + 2C_{12} > 0$ and $C_{44} > 0$), which indicates that the BCC crystal structure remains stable for these compositions. The Poisson ratio and B/G ratio seem to both increase with increasing Ti. Both of these values have been suggested to correlate well with the ductility of a material, implying that higher Ti content improves ductility. Chen *et al.* also indicated that Young's modulus (and hence yield strength) decreases with increasing Ti. To verify the accuracy of these results, the authors compared the properties of the equiatomic composition TiVNbMo to experimental values from literature and found a reasonable consistency.

New fist-principles methods such as Lederer-Toher-Vecchio-Curtarolo (LTVC) have been established over the last five years to provide novel approaches towards calculating solid solution phase stability in HEAs in order to guide future alloy discovery[105]. This method incorporates energy calculations into a mean-field statistical mechanics model, which uses order parameters to predict the transition temperature of a HEA system into a solid solution phase. The authors lay out the development of their protocol in 3 stages: (i) The automatic flow for material discovery (AFLOW)[106] repositories are used to train cluster expansion (CE) models[107] within the Alloy Theoretic Automated Toolkit (ATAT)[108] and estimate zero temperature energy configuration of atomic configurations, which are derivative structures from either FCC or BCC lattices, on which HEAs show solid solution formability; (ii) Then, the estimated atomic configurations are entered into a mean field statistical mechanical model called the generalized quasi-chemical approximation (GQCA)[109]; (iii) Finally, an order parameter is proposed by calculating the evolution of the probability of finding certain ordered configurations of atoms within the lattice.

To test this new method, the authors verified its accuracy by comparing its predictions to Monte Carlo simulations and experimental data for binary alloys. They also compared CALPHAD predictions via Thermo-calc for ternary alloys and experimental data from the literature. Once the method was considered reliable and accurate, the authors used it to predict the solid solution formation in many different alloys. They compared their predictions to the well-known empirical rules that usually inform the design of HEAs to form solid solutions. Figure 6A and B show the plots of the electronegativity and atomic size differences, as well as the VEC and atomic size differences. The large scatter of the green data points suggests that the LTVC method can be used to predict the formation of solid solutions beyond what is typically expected by the usual empirical rules. This study suggests that LTVC shows excellent potential to efficiently explore a large compositional space and discover new alloys that would not be considered under previous knowledge.

As HEAs have been increasingly studied over the past decade, certain empirical rules have been established that correlate well with the observed properties[110]. In the past, it has been suggested that these empirical rules can provide a guideline surrounding the design of HEAs with desirable properties, such as the formation of single-phase solid solutions[111]. However, certain empirical rules, such as the VEC threshold for the stability of FCC and BCC solid solutions, have failed to maintain predictive accuracy over the

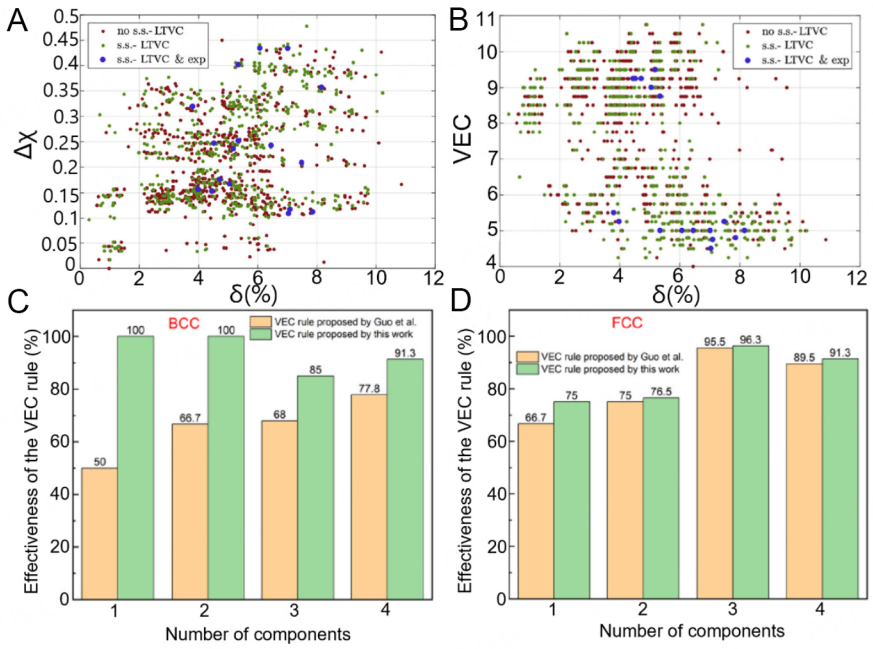

Figure 6. LTVC model predictions for quaternary and quinary alloys (green - predicted SS, blue - predicted SS and verified by experiments) plotted as a function of (A) the electronegativity difference and the atomic size difference; (B) the VEC and the atomic size difference. These figures are quoted with permission from Lederer *et al.*[105], copyright 2018, Elsevier. The effectiveness of the VEC rule previously used and the proposed rule from the work of Yang *et al.* in the Al-Co-Cr-Fe-Ni system[112], copyright 2022, Elsevier; (C) BCC structure (D) FCC structure. These figures are quoted with permission from Yang *et al.*[112], copyright 2022, Elsevier. BCC: body-centered cubic; FCC: face-centered cubic; LTVC: Lederer-Toher-Vecchio-Curtarolo; VEC: valence electron concentration; SS: solid solution.

years[112]. Yang *et al.* revisited this rule using special quasirandom structures (SQS) to investigate 180 compositions within the Al-Co-Cr-Fe-Ni alloy system[112]. The predictions of the phase selection between FCC and BCC were then compared to previous predictions made using the VEC of the alloy system. In their findings, Yang *et al.* argued that the threshold of VEC < 6.87 for the stability of the BCC phase could not accurately predict the phase formation in this system. The results presented by Yang *et al.* suggest that the FCC phase is stable when VEC < 8 and VEC < 5, while the BCC phase is most stable when 5 < VEC < 6.87. This finding reflects more accurately the trends illustrated in their work and is consistent with experimental data. The comparison for the accuracy of the two VEC rules is presented in Figure 6C and D, which shows that the new VEC rule has a superior prediction accuracy for both the BCC and FCC phases when the number of elemental alloy components increases from 1 to 4. It should be noted that this new rule also works well for quinary alloys but does not work well in predicting the dual-phase region. Further study is needed to produce more robust empirical rules that allow for simple rule-of-thumb predictions.

Molecular dynamics

Molecular dynamics (MD) simulations represent a powerful tool to explore and predict material properties of potentially useful materials before significant investments in experimental characterization are made. In MD simulations, the researchers typically define an MD box that outlines the boundary conditions of the system as well as the initial positions and velocities of each atom[113]. The ambient conditions of the simulated system must also be defined, such as temperature and pressure. Once it is initialized, the system is allowed to reach thermal equilibrium[113]. Then the microscopic trajectory of each atom is determined by Newton's equations of motion depending on the potential energy functions utilized in defining the system[113,114]. The accuracy of simulated atom trajectory via MD simulations makes these methods well-

suited to study the nucleation and evolution of defects such as vacancies, dislocations, grain boundaries, and twinning[115-117].

In the past, MD simulations have also been used to explore phase transformation, mechanical behavior, nucleation and crystallization processes within HEAs[118-120]. MD simulations can study much larger systems with faster computation times than ab-initio calculations because they use classical Newtonian mechanics versus the quantum mechanical interactions on which ab-initio methods are typically based. They can also accurately simulate non-equilibrium systems due to the rapid time scales over which a simulation is conducted[113]. Despite these impressive advantages, a known weakness of MD simulations is that their accuracies depend heavily on the accuracy of the potential energy functions used to define them. However, these potential energy functions must first be measured by experimentation or calculated via ab-initio methods, which can limit the applicability of MD simulations to novel systems that have not been studied before[113]. This section presents works that take advantage of the strengths of MD simulations to explore large composition and application spaces with relatively low computation times.

As previously discussed, many computational methods can be used to investigate and predict material properties, such as yield strength, hardness, and phase formation. However, MD simulation has the added benefit of allowing researchers to investigate deformation mechanisms within an alloy via simulation of atomic motion under various ambient and loading conditions[118]. This ability is especially important as it is very difficult and laborious to observe plastic deformation processes under experimental[118,121]. Pan *et al.* applied atomic-scale tensile MD simulations to a $Fe_{80-x}Mn_xCo_{10}Cr_{10}$ alloy system to investigate transformation-induced plasticity (TRIP) and twinning-induced plasticity (TWIP) mechanisms in this system[121]. In this work, the atomic fraction of Mn, strain rate, and grain size were all adjusted to investigate each variable's effect on the system's deformation mechanisms[121]. Figure 7A shows a schematic illustration of the model where green dots represent the FCC phase and white dots denote grain boundaries. The FCC transforms into BCC and HCP during deformation, and this transformation was found to be most prevalent when x = 40. The addition of Mn also reduced the stacking fault energy, which facilitated twinning during deformation, leading to improved strain hardening. Interestingly the transformations and twinning mechanisms were suppressed for smaller nano-grain sizes, which Pan *et al.* attributed to the transformation from the intragranular evolution mechanism at larger grain sizes to the intergranular evolution mechanism at smaller grain sizes. This study shows the potential of MD simulations to explore compositional space and to provide a detailed analysis of deformation mechanisms before significant investments in experimental characterization.

MD simulations can be used to investigate the relationship between the stacking fault energy and strengthening mechanisms within an alloy system. Understanding this relationship can then provide guidelines for designing new HEAs with tailored properties and deformation mechanisms suited to specific applications[122]. Jarlov *et al.* performed MD simulations using the Large-scale Atomic/Molecularly Massively Parallel Simulator (LAMMPS) to investigate the effect of the chemical composition in the Co-Cr-Fe-Ni alloy system on the generalized stacking fault energy (GSFE)[122]. The authors used this method to explore the system's strengthening and deformation mechanisms during tensile tests. Figure 7B shows the simulated cell, and the planes marked as I, II, and III indicate the planes displaced during the tensile simulation. Based on the simulations, it was found that increasing Ni and Co contents led to an increase in the energy required to introduce stacking faults and deformation, while increasing Cr and Fe contents led to a decrease in the energy required to introduce these defects. When carrying out tensile simulations of the various compositions, it was found that the yield strength correlated linearly with the energy required to introduce intrinsic stacking faults. Thus, the strongest composition was identified as $(CoCrNi)_{90}Fe_{10}$,

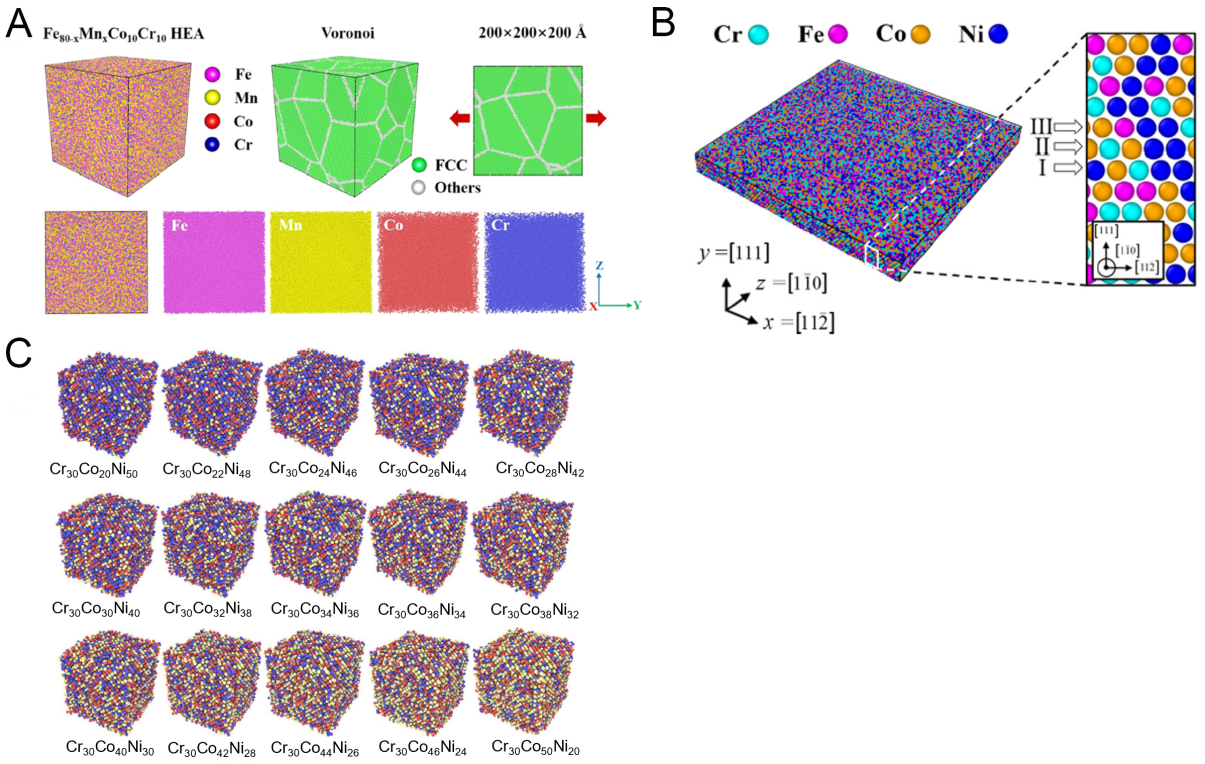

Figure 7. (A) Constructed molecular dynamics model of $Fe_{80-x}Mn_xCo_{10}Cr_{10}$ HEAs with FCC lattice structure and distribution of elements in the model. This figure is quoted from Pan *et al.*[121], copyright 2022, Elsevier; (B) simulation cell used in LAMMPS to calculate generalized stacking fault energy of the Co-Cr-Fe-Ni system. This figure is quoted with permission from Jarlov *et al.*[122], copyright 2022, Elsevier; (C) elemental distribution in the Co-Cr-Ni MEA system with different compositions produced by MD simulation. This figure is quoted with permission from Li *et al.*[123], copyright 2021, Elsevier. FCC: Face-centered cubic; HEA: high-entropy alloy; MD: molecular dynamics.

achieving the highest number of deformation twins. This result illustrates the power of MD simulations to optimize the alloy composition based on yield strength and tailoring of the simulated deformation mechanism.

While MD simulations can be powerful tools to predict the material properties of alloys, the high computational cost associated with these simulations makes it difficult to rapidly produce large datasets for high-throughput studies[123]. On the other hand, ML techniques are known for their potential to quickly and efficiently process and output huge amounts of data and thus offer a means to overcome the low data output of MD simulations. Li *et al.* combined high throughput MD simulation with ML to leverage both techniques' strengths to explore an extensive data set and provide accurate and detailed information on the material properties[123]. MD simulations can produce highly accurate predictions of yield strength, but the data produced by these simulations have high dimensional input-low dimensional output characteristics. These properties make it challenging to produce mathematical models to predict the correlation between input factors and yield strength. On the other hand, ML techniques can produce enormous amounts of data. Still, their accuracy requires a large and robust set of training data that experimentation cannot do. Thus, Li *et al.* utilized high-throughput MD simulation to produce an extensive training data set to train an ANN that can almost fully explore the composition space of the Co-Cr-Ni medium entropy alloy (MEA) system[123]. Figure 7C shows examples of different MD simulation models prepared for this study. The predictions made by the ANN were shown to be highly accurate. This work highlights the potential for high throughput MD simulations used in tandem with ML techniques to produce vast amounts of highly

accurate data that can efficiently identify optimal compositions within a large composition space, thereby overcoming the inherent weakness in each technique by leveraging the strengths of the other. Applying this method to other combinations of computational techniques may offer researchers new opportunities to expand the computational speed, size, and accuracy of future computational studies, which can accelerate alloy discovery far beyond the current state-of-the-art results.

The use of combining MD simulations with ML techniques was also explored by Zhang *et al.* to explore the non-equiatomic compositions within the Fe-Co-Cr-Ni-Mn alloy system[124]. In this case, the deformation of 100 compositions with a single-crystal structure was simulated in three different crystallographic directions, [100], [110], and [111]. The simulated stress-strain responses of these compositions are shown in Figure 8A. Three different ML techniques were then used to predict further the yield stress of non-equiatomic compositions within the alloy system. Unlike other ML tasks, the authors of this work used ML techniques to carry out binary classification of "Good" and "Weak" yield strength rather than quantitative prediction of yield strength. The advantage of this method is that ML programs trained with simulations of single crystals can be used to find optimized compositions that show promise as polycrystalline structures. Typically, polycrystalline models are much larger than single-crystal ones, which can make them more computationally expensive[125]. By leveraging the ability of ML classification techniques and the computational efficiency of high-throughput MD simulations of single crystals, the authors can produce highly efficient means to rapidly identify candidates for optimized compositions of HEA space. This technique was used again by Zhang *et al.* to carry out similar classification predictions for the Cu-Fe-Cr-Co-Ni alloy system[124]. It was again shown to be highly accurate and efficient at pointing out candidates with optimal yield strength[126]. This approach significantly refines the potential compositional space that experimentation needs to explore.

While MD simulations are useful in exploring the compositional space of a system, they can also be used to study material performance within other design dimensions, such as application temperature. Jian *et al.* used MD simulations to study the effect of aluminum concentration, temperature, and strain rate in amorphous $Al_xCoCrFeNi$ HEAs to study their potential as low-density structural materials[127]. Figure 8B shows the stress-strain curves of two of the three simulated compositions ranging from 300 K to 1,200 K. For all three compositions, the yield strength and Young's modulus both strongly depended on the temperature rather than the Al content. The temperature dependence of the yield strength originated from the high migration ability of atoms at higher temperatures, especially at 1,200 K, which was above the simulated glass transition temperature of about 1,100 K. The authors also varied the strain rate from 10^8-10^{11}/s and found that the yield strength and Young's modulus increased with increasing the strain rate. The authors explained that a higher strain rate leads to a larger free volume but that at high strain rates, the times required for free volume rearrangement and atomic diffusion increase greatly. This relationship between free volume and atomic diffusion causes the effective free volume conducive to atomic migration to decrease. Thus, the atomic motion is impeded, which leads to increased strength. This study highlights the flexibility of MD simulations to explore compositional space and various ambient and application conditions that can provide a more holistic understanding of material performance.

CALPHAD calculations

Phase diagrams are geometric representations of alloy systems under thermal equilibrium and typically denote the boundaries of composition and temperature where phase transformations are expected to occur[14]. These diagrams form the basis for studying solidification, crystal growth, and solid-solid phase transformations. Since the 1970s, the calculation of phase diagrams has become an integral part of alloy design, specifically through CALPHAD technology[14]. The technique relies on the minimization of the total Gibbs free energy of the system using the temperature, pressure, overall composition, and Gibbs energy function stored in databases[128].

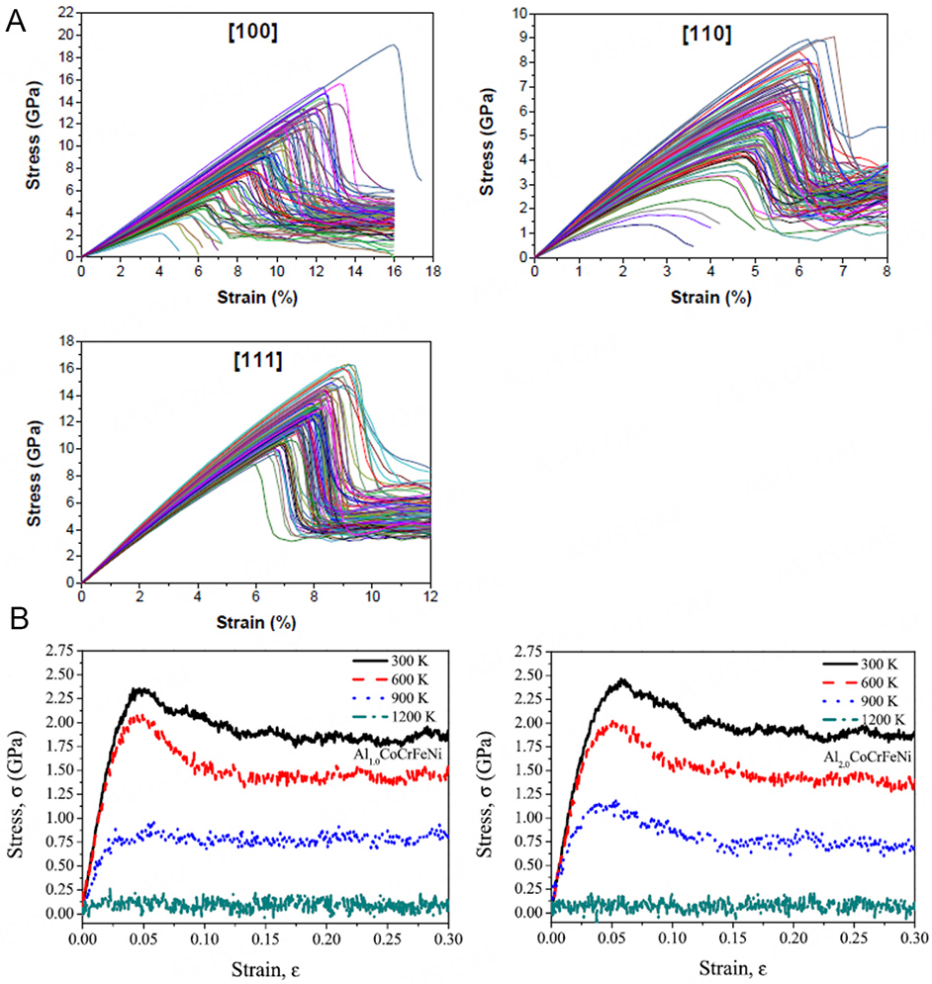

Figure 8. (A) MD simulated stress-strain response of single-crystal Fe-Co-Cr-Ni HEA system with different compositions (all elements are adjusted from 5 at. % to 35 at. %) loaded in different directions. This figure is quoted with permission from Zhang *et al.*[124], copyright 2021, Elsevier; (B) MD simulated stress-strain response of amorphous $Al_xCoCrFeNi$ (x = 1.0 and x = 2.0) HEAs at different temperatures. This figure is quoted with permission from Jiang *et al.*[127], copyright 2022, Elsevier. HEA: High-entropy alloy; MD: molecular dynamics.

The selection of the appropriate database is crucial for accurate calculations as the database should at least cover all the constituent binary and ternary sub-systems to provide accurate phase predictions for complicated alloy systems[129]. It should be noted that a current bottleneck in the field is the lack of comprehensive thermodynamic databases which cover large compositional and temperature spaces. Future experimental works are needed to help fill this gap. Recently, even first principle calculations have shown promise to build such databases with less effort than required for experimental characterization[129]. The current section provides examples of works that take advantage of the computational efficiency of CALPHAD methods to rapidly explore huge compositional spaces, which can reduce the large compositional spaces to ones that can be feasibly explored by experimentation.

One of the pioneering works to tackle the issue of combinatorial high-throughput studies using CALPHAD is carried out by Senkov *et al.*[130]. In this study, the authors used 9 different CALPHAD databases to

calculate every equiatomic alloy containing 3-6 elements out of 26 elements[130]. This calculation resulted in screening 130,000 different alloy compositions to predict the phases at both their melting temperatures and 600 °C. Interestingly, Senkov *et al.* found that the proportion of alloys with solid solution (SS) microstructures decreased as the number of components increased, as seen in Figure 9A[130]. This contradicts the general notion that increasing the number of elements would increase the configurational entropy and thus promote SS formation. In order to investigate the cause of this discrepancy, Senkov *et al.* calculated the entropy of mixing (ΔS_{mix}) and enthalpy of mixing (ΔH_{mix}) for each composition which describes the Gibbs free energy for SS phases. They also calculated the entropy of formation (ΔS_f) and enthalpy of formation (ΔH_f) for the intermetallic (IM) phases in each composition using CALPHAD. Then they used the entropy and enthalpy change of the different predicted phases to calculate the minimized Gibbs free energy to obtain quantitative predictions of the phase formation within each composition and compare them to reported phases in the experimental literature.

Through the previous analysis, they explained that the configurational entropy increases with ln(N), where N is the number of elements, while the possible binary interactions increase with (N/2)·(N-1). Thus, the number of binary interactions increases much faster than the configurational entropy, which increases the likelihood that an IM phase with a highly negative enthalpy of formation exists within a HEA system. Thus, the Gibbs free energy of possible IM phases decreases more rapidly than that of solid solution solutions as the number of elements increases. This work highlights the ability of large computational datasets to allow us to re-evaluate our fundamental assumptions of alloy design by providing large statistical datasets that reveal trends that may not be obvious from experimental testing.

Although many HEAs have been reported to form SS phases at lower temperatures, these are often metastable due to the inherent sluggish diffusion in HEAs. The fast computational speed of CALPHAD methods allows researchers to rapidly screen the composition phase for compositions that maintain a SS as the stable equilibrium phase even at low temperatures. Such methods have been utilized to predict the stable phases of 3 million compositions in 4 different alloy systems of AlCrMnNbTiV, AlCrMoNbTiV, AlCrFeTiV and AlCrMnMoTi[131]. This process was enabled by running approximately 100 calculations in parallel on single CPU cores in a computing cluster. This study aimed to identify various compositions that form single-phase solid solutions (SPSS) at low temperatures and then design compositions that are likely to exhibit good oxidation resistance. By incrementally adjusting the contents of various elements, the authors were able to investigate the effect of each element on the stability of SPSS. The alloy systems shown to have the most significant number of SPSS compositions were the AlCrMnNbTiV and AlCrMoNbTiV systems. Figure 9B shows the 2D projection of the compositional space explored in the AlCrMoNbTiV, where each red dot represents a composition with a predicted single-phase BCC microstructure. It was found that placing constraints to limit the Al and Cr contents can improve SPSS formation, as seen in the top 2 rows of Figure 9B but lowers the oxidation resistance. Thus, the optimal compositions found near the center of the high SPSS formation region and still maintaining a high oxidation resistance were $Al_{25}Cr_7Mn_{25}Nb_1Ti_1V_{41}$ or $Al_{21}Cr_7Mn_{21}Nb_1Ti_9V_{41}$. This study highlights the ability of high throughput CALPHAD methods to reduce a massive design space of over 3 million compositions down to a handful of promising candidates that can feasibly be explored even using conventional manufacturing methods.

The equiatomic Cantor alloy (CoCrFeMnNi) has been studied extensively in the past, including its deformation mechanism, phase formation, and mechanical properties at varying temperatures[132-134]. However, the non-equiatomic compositions have not been explored as deeply[135]. Assuming that a 1 at. % increment in any element's atomic fraction constitutes a new alloy then the compositional space for a generic 5-element alloy system covers an excess of 10^6 unique compositions. Thus, CALPHAD or ML

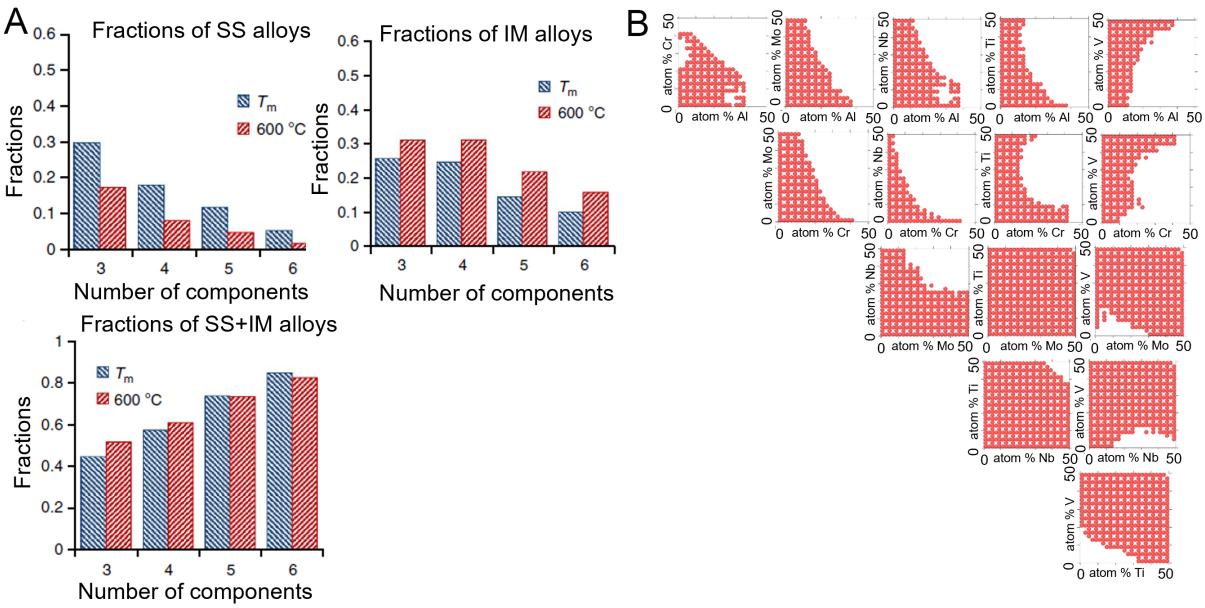

Figure 9. (A) Fractions of CALPHAD predicted single-phase solid solution, intermetallics, and solid solution and intermetallic equimolar alloys in 3 to 6 component alloy systems at the melting temperature (T_m) and at 600 °C. This figure is quoted with permission from Senkov *et al.*[130]; (B) two-dimensional projection of $Al_aCr_bMo_cNb_dTi_eV_{1-a-b-c-d-e}$ phase diagram from CALPHAD showing compositions within two-dimensional space where a BCC solid solution phase forms at 800K. This figure is quoted with permission from Klaver *et al.*[131]. IM: Intermetallic; SS: solid solution.

models are the best methods to screen through the massive composition space. However, the experimental databases on this system lack size and detail, and thus a ML approach cannot be adequately trained. For this reason, Conway *et al.* used high throughput CALPHAD methods to design composition within the Cantor alloy system (Co-Cr-Fe-Ni-Mn) that possesses a combination of high SPSS stability, good mechanical properties, and low material cost[135]. The high-throughput screening analyzed 1.78 million compositions where the elemental contents were gradually incremented by 1-2 at. % interval step. The phase fractions were calculated every 50 K between 500 K to 2,500 K to screen for compositions that produced thermally stable SPSS. Further constraints were applied to ensure every element was present in at least 10 at. %, and the Co and Ni contents were limited to 15 and 20 at. % to reduce the cost of the alloys. Twinning-induced plasticity (TWIP) and solid solution hardening (SSH) were fundamental strengthening mechanisms within this system. Thus, the authors used parameters within the TC-HEA database for their CALPHAD calculations of the SSH values and stacking fault energies (SFEs) for the screened compositions. Figure 10A shows the SFE and SSH plots in a quaternary diagram where the Co content was assumed constant at 10 at. %. The red circle illustrates the composition chosen by the authors ($Co_{10}Cr_{12}Fe_{43}Mn_{18}Ni_{17}$), while the red stars indicate the optimal composition using only the SFE or SSH as the guiding parameter. The composition explored showed only slightly lower yield strength than the equiatomic Cantor alloy at room temperature but showed high strength and ductility at elevated temperatures and exhibited a 40% reduction in cost compared to the equiatomic Cantor alloy. Based on these results, future thermodynamic screening for alloys can incorporate the strengthening mechanisms and material cost into complex alloy design.

The process-structure-property-performance (PSPP) relationship is the central paradigm in materials science. The fundamental goal of many materials scientists is to use computation, theory and experimentation to establish causal trends between the individual elements of PSPP to systematically achieve better material performance. To that end, Abu-Odeh *et al.* contextualized alloy design as an inverse phase stability problem (IPSP)[136]. IPSP is defined as the need to identify the set of thermodynamic

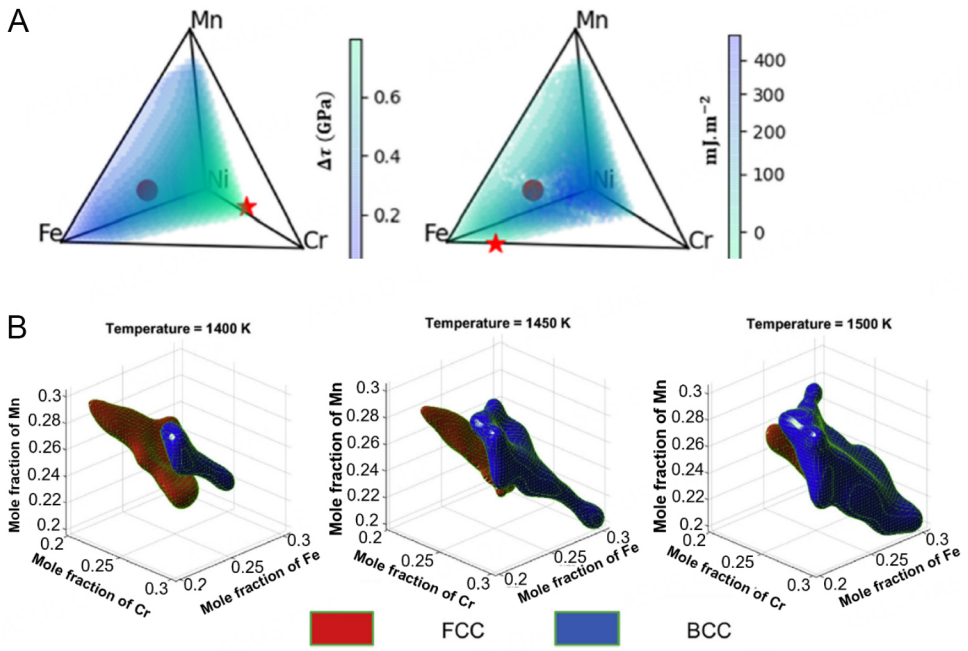

Figure 10. (A) Quaternary phase diagrams at fixed 10 at. % Co illustrating explored composition space. The red circle points out the composition that is experimentally tested, and the red stars indicate the target compositions to maximize hardness (left) and minimize stacking fault energy (right). This figure is quoted with permission from Conway *et al.*[135]; (B) CSA predicted single-phase solid solution compositional spaces for FCC and BCC at 1,400 K, 1,450 K, and 1,500 K. This figure is quoted with permission from Abu-Odeh *et al.*[136], copyright 2018, Elsevier. BCC: Body-centered cubic; CSA: constraint satisfaction algorithm; FCC: face-centered cubic.

conditions that lead to the stabilization of desirable phases which produce high-performance materials. One such example is to provide the coordinates composition and temperature space that result in SPSS for HEAs. The approach Abu-Odeh *et al.* took to tackle this problem is described as a constraint satisfaction algorithm (CSA) which involves the use of ML protocols executed in tandem with CALPHAD calculations to satisfy specific material property criteria/constraints.

This method enables efficient exploration of a large composition region to identify regions of arbitrarily complex phase constitution characteristics. This approach has the potential to design alloy compositions of any phase fraction rather than just focusing on the discovery of SPSS, as previously shown in other works. Abu-Odeh *et al.* applied their framework to the Cantor alloy (Co-Cr-Fe-Ni-Mn) system, where they explored the regions of SPSS stability for both FCC and BCC phases. Figure 10B visually represents the change in FCC and BCC stability with increasing temperature for a ternary sub-section of the compositions explored. After confirming the outcomes of the SPSS regions in the quinary compositions of the system, the approach was expanded to search for precipitation hardening compositions in the Al-CoCrFeNi system by identifying composition regions that include minor secondary phases. It was expressed that the secondary phase would only be considered if it did not form via spinodal decomposition, as this would not lead to any significant precipitation hardening. With this technique, the authors could identify composition spaces most likely to exhibit precipitation-hardening behavior. They highlighted that providing more detailed constraints can further refine the predicted composition space to provide a target region that can be practically explored via experimental methods.

Comparison of computational methods

The previous categories of computational methods all serve important functions in the process of predicting and narrowing the huge compositional space of HEAs. To ensure efficient usage of computational resources

and time, it is crucial for researchers to understand which method is most useful for their individual applications. This section offers a direct comparison between their individual strengths and weaknesses based on the previously discussed studies.

ML techniques have numerous advantages that researchers can use to explore many compositions at once. Firstly, the computational efficiency of most ML methods allows some studies to screen up to 10^5 compositions in a reasonable time frame[90,137]. The faster computation speed of ML than other computational techniques makes it particularly suited to exploring large composition spaces. Additionally, the ability to select various combinations of features as input variables, such as composition, atomic radius, valence electron concentration etc., gives ML a significant advantage in versatility allowing for pattern recognition between features that would normally not be possible with the human mind[82,138,139]. Despite the impressive capabilities, ML techniques rely heavily on large robust datasets to generate useful models[81,90,139]. Unfortunately, the relatively young age of the field of HEAs and the vast composition space means that the relative size of the currently available datasets is still quite small[48]. The small datasets limit the compositional regions where accurate ML models can be trained and applied[81,82]. The other common criticism of ML models is their lack of interpretability. ML models essentially act as a computational black box, meaning that even when they provide accurate predictions, the underlying physics is obscured by the complicated statistical calculations that are performed, making it difficult to build useful intuition from such models[78,79,87,140].

In contrast to the ML models, both first-principles and MD simulation methods rely primarily on well-known quantum mechanical and classical laws instead of statistical models[114,117,138]. This ensures that a strong fundamental understanding of the predicted properties can be extracted from such models. The reliance on fundamental physics also reduces the need for large training datasets as the required datasets are often already contained in readily available databases[125,141]. MD simulations also have the added benefit of illustrating the dynamic evolution of microstructures during an experiment, thereby providing atomic scale information on the phase transformation and deformation of materials during usage, which cannot be achieved using any other computational technique[127,142]. However, both first-principles and MD simulation methods are much more computationally expensive than ML and CALPHAD methods[138]. Thus, first-principles and MD techniques cannot explore as many compositions as ML and CALPHAD methods as seen in Table 1, where first-principles and MD can screen up to 10^4 and 10^3 compositions, respectively.

Recent studies have attempted to overcome this flaw by combining first-principles calculations with ML to produce models that are computationally efficient and highly accurate and provide physical insight into chemical segregation and phase formation[143-145]. Leong *et al.* used a cluster expansion (CE) model, which expands the configurational energy of an alloy structure in terms of various atomic clusters[144]. This model was trained using data obtained through first-principles calculations. Once the configurational energy is calculated for the clusters in the test set, the authors calculate the probability of the nearest neighbor (NN) atomic pairing between the different atomic species in a Mo-V-Nb-Ti-Zr alloy system to predict the Warren-Cowley short-range order (SRO) parameters[144,146]. This SRO allows the authors to highlight the tendency of Zr to segregate and cluster leading to the formation of intermetallic phases below 1,400 K and single-phase solutions above 1,400 K.

Finally, CALPHAD methods are both computationally efficient and have sufficiently large databases to produce accurate predictions for many HEA compositions[147,148]. In fact, CALPHAD methods are able to screen more compositions than any of the other computational methods (up to 10^6 compositions) in a reasonable time span[135]. Despite this large computational efficiency, CALPHAD methods can only provide

Table 1. Comparison of pros, cons, and capabilities of various computational methods

Computational method	Predicted Properties	Pros	Cons	Number of screened compositions	References
Machine learning	Elastic constants Phase formation Phase transformation temperature Hardness Tensile strength Compressive strength	High computational efficiency Versatility in predictive features	Requires large training sets Lack of physical interpretability Only gives statistical understanding	10^5	[48,78,79,81,82,87,90,137-139]
First-principles	Elastic constants Phase formation Phase transformation temperature	Low input information needed Provides fundamental understanding Atomic scale detail	Computationally expensive Time-consuming	10^4	
Molecular dynamics	Elastic constants Phase formation Phase transformation temperature Hardness Tensile strength Compressive strength	Provides fundamental understanding Atomic scale detail Dynamically simulate microstructure evolution	Computationally expensive Time-consuming Cannot provide macroscopic results	10^3	[114,115,125,127,141,142]
CALPHAD	Phase formation Phase transformation temperature	High computational efficiency High accuracy Easily interpretable	Only predicts equilibrium conditions No kinetic information	10^6	

information about equilibrium phase formation and transformation temperatures which may not be representative of manufacturing or application conditions. This limitation is especially important for HEAs,c where sluggish diffusion limits the kinetics within the system, which can often lead to the formation of metastable phases that may not be expected under equilibrium conditions.

COMBINATORIAL ADDITIVE MANUFACTURING TO EXPLORE LARGE COMPOSITIONAL SPACE

After narrowing a target composition space using computational methods, the remaining candidate compositions are still too numerous to reasonably explore via traditional metallurgical techniques. Thus, high-throughput manufacturing techniques are needed to rapidly produce samples that cover the candidate composition region. Previous studies have utilized magnetron sputtering and diffusion multiples to produce combinatorial libraries[28,149-151]. However, as previously discussed, these techniques produce samples at micro- or nano-scale, which may not be representative of bulk materials.

Additionally, the cooling rates experienced during magnetron sputtering are orders of magnitude greater than the cooling rates in traditional manufacturing settings[35,36]. Thus, there is a need for a manufacturing technique that can produce vast compositional libraries at a bulk length scale with practically relevant cooling rates. Laser additive manufacturing (LAM) has shown great promise towards that end. Previously LAM has been used to produce alloys with improved properties compared to their conventionally manufactured counterparts[36,152-159]. Two main types of LAM are used in combinatorial studies, i.e., laser directed energy deposition (DED), also known as laser engineered net shaping (LENS), and laser powder-bed fusion (L-PBF)[160]. The DED process utilizes a carrier gas that allows the powder to flow continuously while shielding it from oxidation during deposition. A laser source simultaneously heats the material upon contact with the printing substrate or previous layer[37]. In the case of L-PBF, a flatbed of powder is deposited on a substrate. A laser is then used to melt the particles in a pattern determined by design software to form a part layer by layer[161].

Functionally graded materials

LAM can produce compositionally graded materials, making it a powerful tool for rapid combinatorial material exploration[160]. DED is the more common method used to produce graded materials, as the multiple nozzles can be coaxially aligned with the laser, ensuring that each nozzle's flow rate can be individually adjusted to spatially control the deposited alloy composition[162,163]. By dynamically changing the flow rate during AM, a compositional gradient can be formed, allowing for the exploration of a large compositional space within the same sample [164,165]. This method is schematically illustrated in Figure 11A, where a compositionally graded wall is produced starting from pure Cantor alloy at the base and increasing the content of refractory metals with increasing the build height[166]. Pegues *et al.* used this method to add Nb, Ta, and Ti6Al4V to CoCrFeMnNi to produce 3 different materials libraries[166]. They explored the effect of these additions on the microstructure and mechanical properties of the resulting alloys. Utilizing this method allowed them to efficiently explore a large compositional space without producing large samples. Micro-hardness tests on all three libraries revealed that the addition of the refractory elements resulted in increased hardness, likely due to the formation of secondary intermetallic phases such as a Laves phase[166].

While DED is the most common method to produce gradient materials compositionally, Wen *et al.* used L-PBF to produce a gradient material, as shown in Figure 11B[167]. Normally, L-PBF is considered undesirable for compositionally graded materials as the powder composition cannot be systematically controlled once loaded in a chamber. Wen *et al.* addressed this issue by adding a partition within the powder hopper so that two different powders could be loaded together. Then a mixer is placed below the hopper that mixes powders along the width of the mixer. This mixture forms a compositional gradient in the laser scan plane when the powder bed is deposited. Thus, a horizontal compositional gradient forms rather than the typical vertical gradients achieved in DED combinatorial studies[168-170]. Wen *et al.* used CoCrFe medium entropy alloy and Inconel 718 as the feedstock powders to prove this new technique's concept. At the pure CoCrFe end of the alloy gradient, a pure FCC phase structure was formed and as the Ni content increased due to the addition of Inconel 718, a secondary HCP phase was formed. The HCP phase content increased with increasing Ni content. The decrease in hardness occurred with increasing Ni-content, which is likely due to the larger sub-grain size observed near the Inconel 718 end.

Li *et al.* used DED to explore the effects of compositional and cooling rate changes on the microstructure and mechanical properties of the Al-Co-Cr-Fe-Ni alloy system [171]. First, they produced a pure CoCrFeNi substrate via casting. Then, they deposited varying amounts of Al on the substrate using a LENS system which formed different compositions of $Al_xCoCrFeNi$ along the substrate surface, ranging from x = 0.51 to x = 1.25, as shown in Figure 11C. The laser was also used for remelting straight lines parallel to the compositional gradient with different laser powers and scan speeds which induced different cooling rates in the compositional library. Three compositions from the library were also chosen to produce casting counterparts to achieve cooling rates far below what is achievable through DED. This method allowed the cooling rate to be varied from 25-6,400 K/s. Their findings showed that the lowest Al-containing compositions exhibited a dual-phase FCC + BCC structure which transitioned to a pure BCC/B2 at near equiatomic compositions. Additionally, compositions with low Al content showed a primary FCC phase with a cellular microstructure. The cellular microstructure followed a power law of the form $\lambda = A \cdot \dot{T}^{-1/3}$ where λ is the cell size, A is a fitted parameter, and $\dot{T}$ is the cooling rate. The microstructure refinement resulted in hardening following the Hall-Petch relationship. This work illustrates the potential for laser-based AM methods to rapidly and simultaneously explore the effects of composition and cooling rate on the phase evolution and mechanical properties of HEAs.

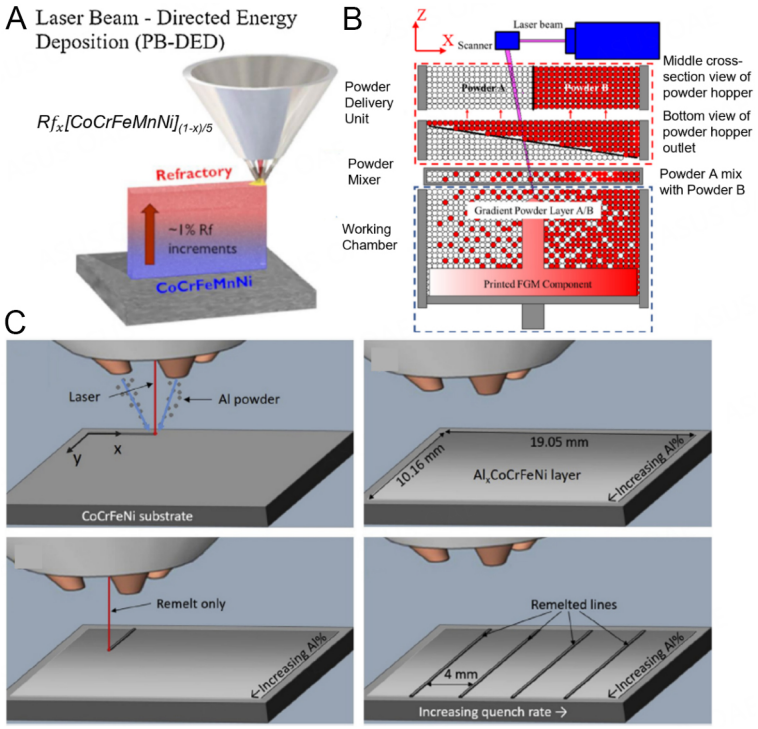

Figure 11. (A) Schematic illustration of high-throughput manufacturing of HEAs in a graded material under laser-directed energy deposition (L-DED). This figure is quoted with permission from Pegues *et al.*[166], copyright 2021, Elsevier; (B) schematic illustration of manufacturing a graded material under laser powder bed fusion (L-PBF) conditions. This figure is quoted with permission from Wen *et al.*[167], copyright 2021, Elsevier; (C) graded material library produced via L-DED in $Al_xCoCrFeNi$. The graded HEA library is remelted to investigate the effects of composition and cooling rate. This figure is quoted with permission from Li *et al.*[171], copyright 2020, Elsevier. HEA: High-entropy alloy.

Teh *et al.* used DED to produce compositionally graded pillars within the Co-Fe-Ni alloy system[172]. By adjusting the content of each element along the build direction, the phase fraction of FCC *vs.* BCC was varied from pure BCC at the base of the pillar to dual phase FCC + BCC to pure FCC at the top. The hardness also varied with build height due to changes in composition and grain size caused by increasing the Ni concentration. They characterized the functional properties of each composition in addition to the mechanical properties by measuring the saturation magnetization, coercivity, and electrical resistivity. After analyzing the combination of properties, the authors presented a radar chart comparing some promising compositions to pure Fe, as shown in Figure 12A.

Gwalani *et al.* varied the V content in an $AlMoCrFeV_x$ (from x = 0 to x = 1) HEA system [Figure 12B][173]. The addition of V led to solid solution hardening, increasing the hardness monotonically from 485 HV at x = 0 to 581 HV at x = 1. The microstructure remained purely BCC for all compositions and remained stable after annealing at 1,100 °C for 30 min. The grain size was also negligibly changed, which indicated high thermal stability. Zhao *et al.* blended Ti and CoCrFeNi powders in various compositions[174]. They then layered the different compositions within a powder supply bin to build a compositionally graded pillar by increasing the Ti content along the build direction[174]. All compositions showed an FCC structure primarily with minor BCC, Laves, and phases that contain Ti. Figure 12C shows a hardness map based on the results taken from the printed graded structure. As the secondary phase volume fractions increased, the hardness increased, and analysis of the various strengthening mechanisms suggested that the inclusion of the secondary phases was the main cause of the increase in strength. However, high Ti content layers also showed significant cracking. Thus, the authors concluded that 10 at. % was the maximum threshold of Ti content to produce crack-free samples and parts in CoCrFeNiTix HEA system.

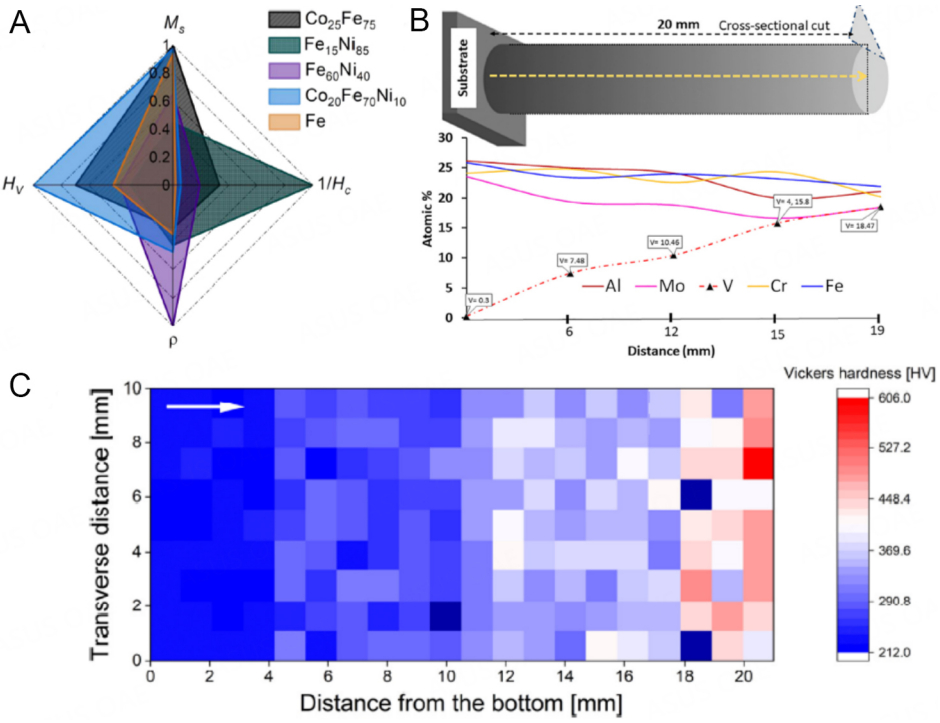

Figure 12. (A) Radar chart comparing properties of various promising compositions discovered from graded material library of the Co-Fe-Ni system. This figure is quoted with permission from Teh *et al.*[172], copyright 2022, Elsevier; (B) change in V concentration along the build direction for $AlMoV_xCrFe$ alloy. This figure is quoted with permission from Gwalani *et al.*[173], copyright 2019, Elsevier; (C) vickers hardness map of the side surface of graded $CoCrFeNiTi_x$ HEA system. This figure is quoted with permission from Zhao *et al.*[174], copyright 2021, Elsevier. HEA: High-entropy alloy.

Bulk materials library

While graded materials provide a convenient means to explore multiple compositions within a single sample, they cannot give a full picture of material performance due to the possible mixing between layers during LAM, which can be difficult to control. In this sense, bulk materials libraries can produce individual samples to be studied in further detail while maintaining a high-throughput approach if rapid characterization techniques can be applied. One such example is illustrated in Figure 13A, where Yu *et al.* used DED to produce a library of bulk samples using elemental Al powder and $Cu_{50}Zr_{50}$ powder in separate powder hoppers, as seen in Figure 13A[175]. This work aimed to find the optimal compositions and processing conditions to produce bulk metallic glass composites (BMGC). BMGCs are materials formed by adding a crystalline phase into a glassy amorphous matrix[176].

The crystalline phase helps hinder the propagation of shear bands and dissipate fracture energy, which can significantly improve the room temperature ductility of BMGCs compared to monolithic bulk metallic glasses[155]. In their work, BMGC samples were deposited and then remelted to produce initially deposited melt pools with similar dimensions and different cooling rates. An 11 × 11 sample library was produced where the Al content was adjusted from 0 at. % to 10 at. % along the x-direction while the laser power was varied along the y-direction from 150 W to 400 W. Finite element modeling (FEM) was used to estimate the cooling rates and XRD analysis was used to confirm the phase constitution. After identifying phases with both amorphous and crystalline phases, the authors defined a uniformity coefficient to estimate the sample that would be expected to show the highest ductility. This criterion arose because ductility is closely related

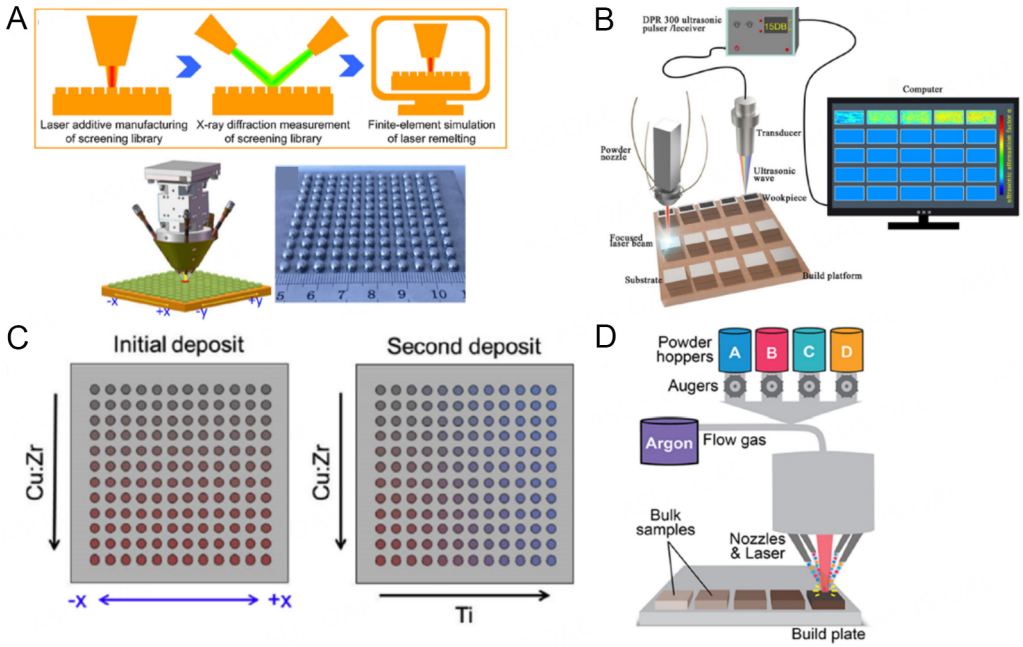

Figure13.(A) Schematic of high-throughput fabrication and screening of combinatorial materials library and images of the printed library of Cu-Zr-Al alloy system. This figure is quoted with permission from Yu *et al.*[175], copyright 2021, Elsevier; (B) schematic of combinatorial material library fabrication and ultrasonic screening to rapidly estimate effective processing parameters of $Zr_{51}Ti_5Ni_{10}Cu_{25}Al_9$ bulk metallic glass (BMG), adapted from Zhai *et al.*[177]; (C) schematic illustration of materials library produced with discrete dots of varying compositions. This figure is quoted with permission from Tsai *et al.*[178], copyright 2016, Elsevier; (D) schematic of DED processing of Fe-Ni-Cr-Mo bulk materials library. This figure is quoted with permission from Islam *et al.*[180], copyright 2021, AIP Publishing. DED: Directed energy deposition.

to the spatial distribution and uniformity of the crystalline dendrites within the glassy matrix. The optimal composition contained 4 at. % Al and used a remelting power of 175 W.

The rapid cooling rates induced by laser-based AM techniques can encourage the formation of amorphous structures in additively manufactured alloys and hence offer a unique opportunity to study bulk metallic glass (BMG) formation[177]. Zhai *et al.* fabricated a library of one composition with varying processing conditions to rapidly determine the optimal conditions to produce a defect-free BMG[177]. The composition used was $Zr_{51}Ti_5Ni_{10}Cu_{25}Al_9$. Using ultrasonic wave attenuation, they were able to rapidly determine the presence of defects, pores, or crystalline grain boundaries that may affect the performance of the BMG. This technique is schematically illustrated in Figure 13B. A laser power of 1,300 W and 600 mm/min was determined to provide the highest fraction of amorphous material while remaining defect-free. This work highlights the use of DED combined with ultrasonic wave attenuation to provide a non-destructive and easy way to rapidly investigate and verify the glass-forming ability of many compositions immediately after they are printed.

It is currently very difficult to predict the glass-forming ability (GFA) of an alloy composition. Thus, the current exploration of BMGs requires a high-throughput investigation similar to that of HEAs. For this reason, Tsai *et al.* deposited a combinatorial library of Cu-Zr-Ti to identify the composition with optimal GFA[178]. Figure 13C shows a schematic illustration of the construction of this library[178]. The library was built by depositing discrete hemispherical samples with varying Cu:Zr ratios between each row of samples. After the initial deposition, a layer of Ti was deposited with various feed rates and simultaneously melted onto the library. Each sample was remelted 2 more times to ensure the elements were fully melted and incorporated into each sample.

Once the library was prepared, each sample was remelted with different laser powers of 200 W, 240 W, and 280 W. Since a higher laser power leads to a lower cooling rate, compositions that maintain glassy microstructure with higher laser power should have higher GFA. Differential interference contrast (DIC) imaging under optical microscopy was used to screen for amorphous materials as samples with amorphous structures show a smooth liquid-like topography under DIC. At the same time, crystalline microstructures appear rough[179]. A total of 144 discrete samples were investigated, and 92 were identified as amorphous for the lowest power. Based on the previously mentioned criteria, the composition with the highest GFA was $Cu_{51.7}Zr_{36.7}Ti_{11.6}$, as it showed a high fraction of amorphous microstructure and was located in the center of the region of compositions that exhibit an amorphous microstructure after remelting at 280 W. It was also pointed out that this method could be extended to alloy systems with even more components by using pre-alloyed powders. Thus, the procedure laid out by Tsai *et al.* illustrates a means to rapidly identify BMGs with excellent GFA within a given alloy system. In addition to the optimal composition, combinatorial studies can also be used to rapidly determine optimal printing parameters for a given alloy system. Islam *et al.* carried out such a study on 25 different compositions in the Fe-Ni-Cr-Mo alloy system to and define a normalized dimensionless parameter based on the energy input density from the laser and the material properties of the constituent atoms[180]. A schematic illustration of their experimental method is illustrated in Figure 13D.

Eutectic HEAs (EHEAs) combine design concepts from both HEAs and eutectic alloys and show great potential for structural applications due to their impressive combination of strength and ductility[156,181]. This combination of properties arises from a hard and soft phase which help provide strength and ductility, respectively. However, further optimization is possible through minor composition adjustments to achieve near-eutectic HEAs. Joseph *et al.* produced a library of bulk $Al_xCoCrFeNi_{2.1}$ samples using the DED method to analyze the effect of Al-content on the microstructure and mechanical properties of alloys with near-eutectic compositions[182]. Figure 14A presents the XRD peak patterns of the compositions explored and shows an increase in the B2 phase with increasing the Al content. Additionally, cast samples with the compositions of each phase were prepared. These allowed the authors to investigate samples with single-phase microstructures that were either purely FCC or purely B2 phase. After analyses of the phase fractions and compressive properties of each composition, it was found that the alloys' yield strength followed a rule of mixtures based on the yield strength of the individual phases. This work highlights the ability of DED to provide large sample sets that allow for rapid characterization of multiple compositions that can elucidate strengthening trends within a system to achieve an optimal composition.

When testing the radiation damage resistance of a material, it is imperative to use bulk samples as the damage layer thickness is typically on the order of microns, and the compositional gradient struggles to maintain chemical homogeneity over large length scales. Additionally, thin-film-based materials typically form nano-grain microstructures, which artificially increase the radiation damage resistance of a material, making the results misleading compared to application conditions. Moorehead *et al.* printed a compositional library of Cr-Fe-Mn-Ni alloys to assess their irradiation properties[183]. It was found that Cr-rich compositions showed an increase in BCC phase fraction, while Fe and Ni-rich compositions showed higher FCC content, and Cr and Ni tended to segregate together preferentially. This trend can be seen in Figure 14B, where the compositions with a higher Cr content show more severe segregation. Nanoindentation was utilized as a high-throughput means to measure the effect of ion irradiation on the hardness of each composition. Radiation-induced hardening was found in all compositions with FCC, BCC, and FCC + BCC phases. The increase in hardness was consistently shown to be 1-1.5 GPa, with BCC-rich

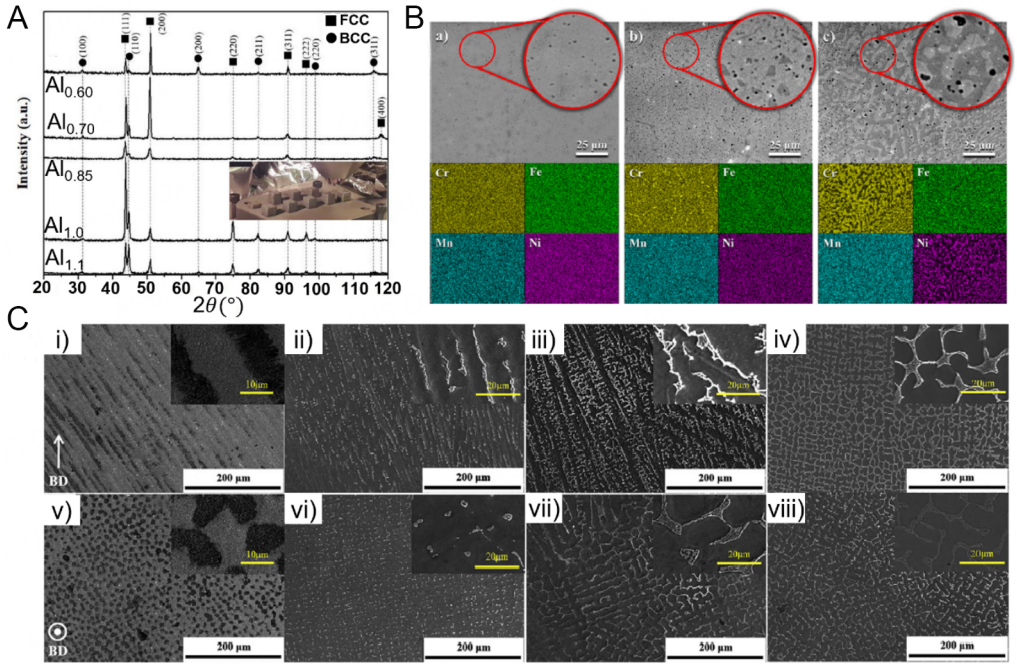

Figure 14. (A) X-ray diffraction profiles of $Al_xCoCrFeNi_{2.1}$ showing the change in FCC and BCC phase fractions with changing Al content. The inset shows an image of material library. This figure is quoted with permission from Joseph *et al.*[182], copyright 2020, Elsevier; (B) SEM images and EDS maps of $Cr_{19}Fe_{31}Mn_{11}Ni_{39}$, $Cr_{28}Fe_{23}Mn_{20}Ni_{29}$, and $Cr_{42}Fe_{17}Mn_{20}Ni_{21}$, from left to right. This figure is quoted with permission from Moorehead *et al.*[183], copyright 2021, Elsevier; (C) SEM images of the as-deposited $CoCrFeNiNb_x$ parallel to the build direction: (i) $CoCrFeNiNb_0$; (ii) $CoCrFeNiNb_{0.1}$; (iii) $CoCrFeNiNb_{0.15}$; (iv) $CoCrFeNiNb_{0.2}$; and perpendicular to the build direction: (v) $CoCrFeNiNb_0$; (vi) $CoCrFeNiNb_{0.1}$; (vii) $CoCrFeNiNb_{0.15}$; and (viii) $CoCrFeNiNb_{0.2}$. This figure is quoted with permission from Zhou *et al.*[9], copyright 2019, Elsevier. BCC: Body-centered cubic; FCC: face-centered cubic.

compositions showing the least increase in hardness. Additionally, Moorehead *et al.* found that compositions with a high Mn content may have a large amount of Mn depletion after homogenization due to the depressed melting point of high Mn-content alloys. Thus, the authors laid out a guideline to keep the Mn-content below 25 at. %. Finally, the time saved using the high throughput AM approach is highlighted compared to the traditional metallurgical approach of melting and casting. The authors state that traditional melting and casting could take up to 1-2 hours per composition compared to the 10 min per composition required by the DED method.

Zhou *et al.* utilized DED to rapidly produce samples with compositions $CoCrFeNiNb_x$ (referred to here as Nb_x)[9]. The authors investigated the mechanical properties of each alloy composition and its correlation to the phase and microstructures present. Figure 14C shows SEM images of 4 compositions (Nb_0, $Nb_{0.1}$, $Nb_{0.15}$, $Nb_{0.2}$) prepared by DED. The top row shows images taken parallel to the building direction, while the bottom row shows images taken perpendicular to the building direction. The authors concluded that the addition of Nb to the CoCrFeNi system led to a transition from a columnar to an equiaxed structure due to the formation of a secondary Laves phase in addition to the primary FCC phase. The Laves phase also caused an increase in yield strength in the $Nb_{0.2}$ composition more than three times that of the Nb-free composition while maintaining a ductility above 10%.

HIGH-THROUGHPUT CHARACTERIZATION TECHNIQUES

While high-throughput computational methods can narrow down the alloy design space and high-throughput manufacturing methods enable rapid fabrication of samples within the design space, high-

throughput experimental methods are needed to characterize the manufactured materials' properties to experimentally verify which set of composition and processing conditions ultimately leads to the target performance. This section focuses primarily on the different high-throughput methods which can rapidly characterize important material properties such as hardness, strength, ductility, phase and composition, magnetic hysteresis, saturation magnetization, and corrosion resistance.

Mechanical property characterization

Mechanical properties such as strength and ductility are crucial to assess the performance of a material for structural applications[184]. A few important criteria exist for a mechanical test considered to be useful for screening HEAs. First, the sample size and microstructure must represent bulk-like conditions[185]. Second, the test should include a dominant tensile component, as real application conditions often include some tensile stresses[185]. Microhardness and nanoindentation tests are the most common approach towards high-throughput screening of structural materials. These methods can quickly and accurately estimate bulk yield strength[185]. Nanoindentation can also offer broad insights into the post-yielding attributes through analysis of the stress-strain curves it produces[186]. The local nature of these two techniques also makes them highly useful in graded materials libraries where many compositions and microstructures can be manufactured in a single sample for rapid screening.

Here two example studies are provided that use microhardness testing to investigate the effect of composition on hardness. Jiang *et al.* produced various compositions of $CoFeNi_xVMo_y$ alloys to test the effects of composition and microstructure on the hardness[187]. This work concluded that an increase in the Mo content led to increased precipitation of the $CoMo_2Ni$-type intermetallic phase. An increase in Ni content increased the FCC solid solution phase and decreased the hardness. Figure 15A depicts the hardness of the various compositions showing that the peak hardness was reached at the composition equiatomic CoFeNiVMo. Pegues *et al.* also used micro-hardness indentation to build a hardness map of a graded Ta_x CoCrFeMnNi sample, as shown in Figure 15B[166]. This map allowed them to rapidly determine the effect of Ta addition on the hardness of this Cantor alloy-based system. Higher Ta contents encouraged the formation of TaNi-rich intermetallic in the interdendritic region, which caused significant increases in hardness.

Although micro-indentation methods can provide reasonable data for screening materials, the most reliable method to investigate material properties is a lab-scale tension test with samples that conform to either the ASTM E8 standard or another equivalent internationally recognized standard. Here the authors of this review present one example from the literature and their own unpublished data to illustrate the typical results that can be achieved in a combinatorial HEA library. Ma *et al.* added Nb to the AlCoCrFeNi system, which led to the formation of Laves phase that increased the strength of the alloy while decreasing the ductility[188]. Tuning the Nb content allowed them to tune the compressive properties [Figure 15C]. This result indicates that the addition of intermetallic forming elements can be used to achieve a wide array of properties that can be optimized for application-specific uses. Following this design philosophy, the authors of this review recently used DED to produce $CoCrFeNiTi_x$ alloys to achieve a composition with improved mechanical properties. The tensile stress-strain curves of our investigated $CoCrFeNiTi_x$ HEAs are shown in Figure 15D. These results show that adding Ti to the base quaternary alloy increases the yield strength while decreasing the ductility until $x = 0.2$. Beyond this threshold, the yield strength and the ductility of the alloy drop simultaneously. It has been well established that the introduction of Ti into the CoCrFeNi system leads to the formation of brittle intermetallic phases that causes decreased ductility and increased hardness and yield strength[189-191]. The drop in yield strength from $x = 0.2$ to $x = 0.25$ is likely a result of defects that occurred during printing due to a higher fraction of brittle phases.

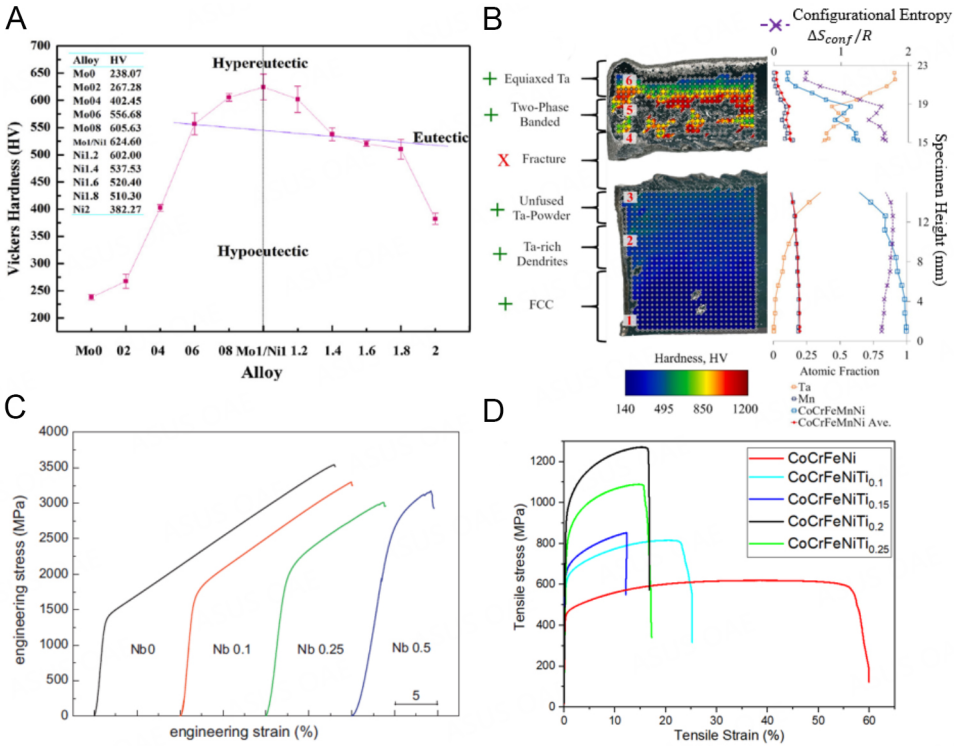

Figure 15. (A) Effects of Ni and Mo on Vickers hardness of $CoFeNi_xVmo_y$. This figure is quoted with permission from Jiang *et al.* [187], copyright 2015, Elsevier; (B) $Ta_xCoCrFeMnNi$ hardness map with associated elemental distribution. This figure is quoted with permission from Pegues *et al.*[166], copyright 2021, Elsevier; (C) compressive stress-strain curves of $CoCrFeNiNb_x$ samples. This figure is quoted with permission from Ma *et al.*[188], copyright 2012, Elsevier; (D) tensile stress-strain curves of $CoCrFeNiTi_x$ HEAs printed in the authors' lab. HEA: High-entropy alloy.

In order to fulfill the rapid testing needs of high-throughput experiments, a high degree of automation must be integrated into the characterization process to decouple experimental progress from the number of hours available to human researchers. To that end, Huang *et al.* developed a high-throughput tensile testing platform to automate the tensile testing procedure and increase the rate and which specimens can be characterized[192]. This method uses a large grip that is held onto the bottom of many dog-bone samples, and this grip is attached to a motorized table that moves the grip laterally into position. A top grip is aligned in the direction of travel, allowing for automated testing of many samples in a small-time frame. In the case of their work, Huang *et al.* tested many samples of 316L stainless steel printed through a combinatorial study of different printing conditions by L-PBF. This platform may also show great potential for combinatorial studies related to the compositions of HEAs by automating tensile testing of compositional libraries produced by laser-based AM.

Phase and composition analysis

XRD is a common tool used to analyze the phases present in a material. The following paragraph illustrates some examples of typical data extracted from XRD analysis in combinatorial studies. Chen *et al.* studied the phase evolution in $(AlCoCrFeNi)_{100-x}Ni_x$ and $(CoCrCuFeNi)_{100-x}Mo_x$ HEAs[193]. XRD analysis shows that when x is between 0 and 4 at. %, both alloys exhibited single-phase solid solution structure where the $(AlCoCrFeNi)_{100-x}Ni_x$ alloy shows a BCC structure and the $(CoCrCuFeNi)_{100-x}Mo_x$ alloy shows an FCC structure. As the Ni content increases, a dual-phase FCC/BCC structure forms, and the FCC phase fraction increases. On the other hand, when the Mo content increases beyond 4 at. %, the FCC/BCC structure also forms, and the BCC phase fraction increases with the Mo content. The XRD patterns of the Ni- and Mo-

doped samples are shown in Figure 16A and B. Moorehead *et al.* used DED to produce a library of Mo-Nb-Ta-W HEAs, which were then examined via XRD[194]. The XRD patterns are shown in Figure 16C. In this case, all the compositions tested showed a full BCC phase.

However, energy dispersive spectroscopy (EDS) analysis showed that Nb was segregated to the interdendritic region. In order to tune the phase structure in a $CoCrFeNiNb_x$ alloy system, our group used DED by placing pre-alloyed CoCrFeNi powder in one powder feeder and pure Nb powder in another. Then, the feed rates from each feeder were adjusted to produce a graded material with increasing Nb along the build direction. The $CoCrFeNiNb_x$ compositions were selected as going from $x = 0$ to $x = 1$, where x was increased by about 0.1 for every 1 mm increase in height. Synchrotron XRD (SXRD) at the Cornell High Energy Synchrotron Source was then performed along the build direction to analyze the phase composition in each region. The beam size was maintained as 0.5 × 0.5 mm such that the measured phase compositions correspond accurately to the designed compositions. As the Nb content increased, an FCC/Laves dual-phase structure formed with the Laves phase volume fraction increased from 0% to 57% as the Nb content increased from 0 to 20 at. %. Figure 16D shows the SXRD results taken for each composition.

In addition to XRD analysis, EBSD can offer a means to probe phases at higher spatial resolution (around 200 nm for EBSD *vs.* about 1 mm for XRD), which may be especially important for gradient compositional libraries where the compositional change can be quite drastic over small length scales[185]. EBSD also has the advantage of being equipped onto SEM facilities. Thus, EDS analysis can often be carried out in parallel such that phase and composition can be resolved almost simultaneously. For experiments that include many phases and samples, there is a need to automate the phase analysis process to make the process more efficient[195,29]. Many groups have used high-throughput SXRD to rapidly identify phases in combinatorial material libraries[196]. The majority of these studies used thin films produced by magnetron sputtering[29,195,197,198]. However, there are almost no studies of large bulk materials that used similar high-throughput methods for phase structure analysis.

It should be noted that a bottleneck for the previously mentioned methods is the human intervention needed during data analysis. This analysis can require impractical time commitments when the number of compositions reaches hundreds or thousands. Thus, the development of automated systems for analyzing XRD, EBSD, and EDS data is crucial to ensure that experimental results of high-throughput experiments can be achieved in a timely manner. Machine learning has recently shown impressive results in this field by correctly indexing phases within an EBSD pattern without requiring human input to guess at the present phases[199]. Although this process has not been attempted for HEAs, it shows great promise to be applied to new materials. Extending this practice further to carry out more in-depth analysis, such as Rietveld refinement for XRD patterns, will greatly accelerate the development of future HEAs.

Magnetic property measurement

Tang *et al.* added Ho to a $FeCoNi(CuAl)_{0.8}$ alloy to investigate the effect of the addition of rare earth (RE) element on the magnetic properties of this system[200]. The initial parent alloy showed a fully FCC structure, and adding Ho led to the formation of a secondary BCC phase. Increasing the atomic fraction of Ho led to an increase in the volume fraction of the BCC phase fraction and no change in the lattice parameter of the FCC phase. As shown in Figure 17A, increasing the Ho content led to lower energy losses via eddy currents and hysteresis until $x = 0.05$. Once $x = 0.07$, the energy losses increased substantially. The decrease in hysteresis loss is due to lower Cu segregation at the BCC-FCC phase boundaries with increasing Ho. This segregation leads to a lower magnetic domain pining effect, decreasing hysteresis losses[200]. At $x = 0.07$, the Cu and Ho tend to segregate heavily to phase boundaries, leading to higher hysteresis losses. The BCC

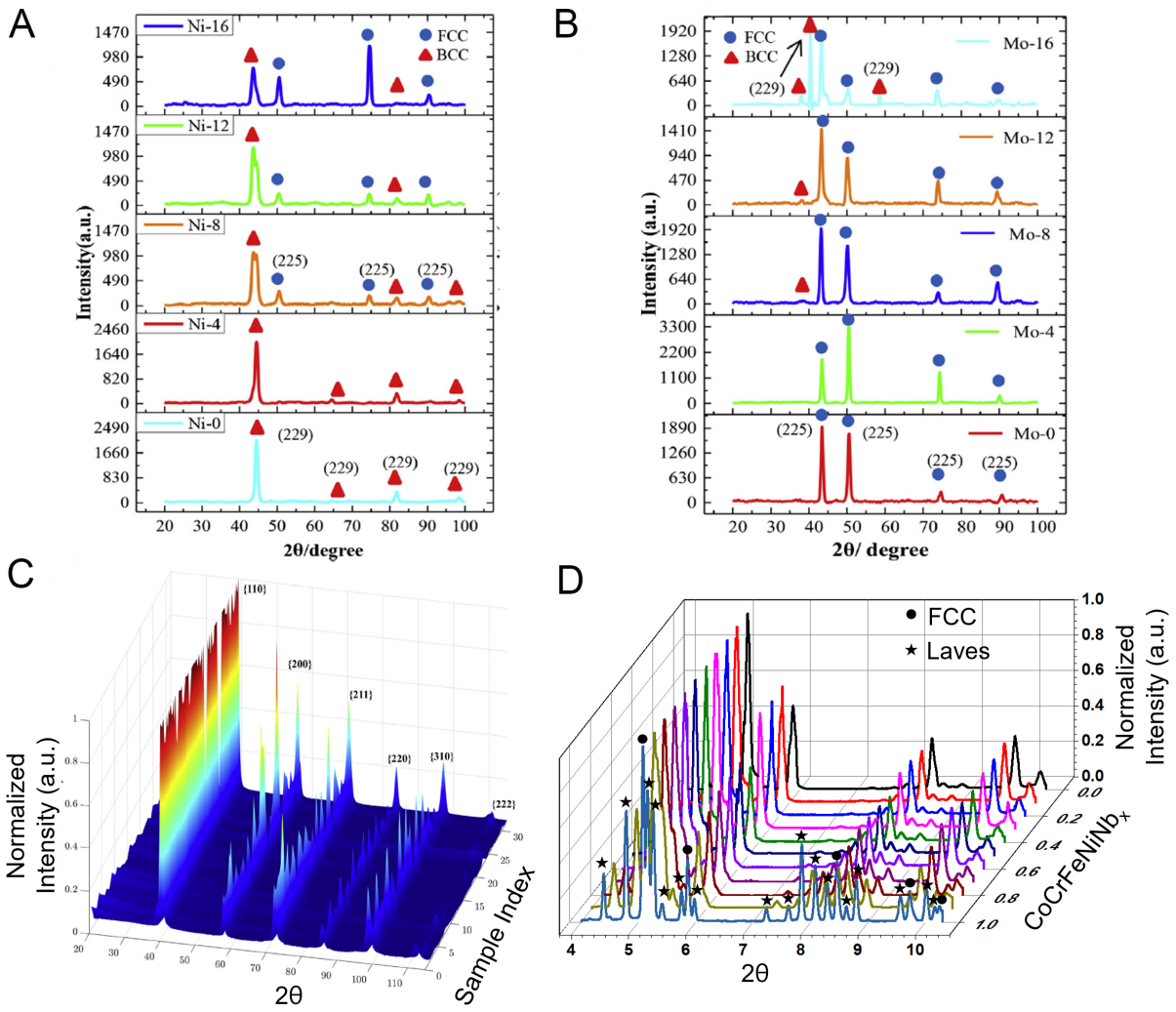

Figure 16. (A) XRD patterns of $(AlCoCrFeNi)_{100-x}Ni_x$. This figure is quoted with permission from Chen *et al.*[193], copyright 2018, Elsevier; (B) XRD patterns of $(CoCrCuFeNi)_{100-x}Mo_x$. This figure is quoted with permission from Chen *et al.*[193], copyright 2018, Elsevier; (C) XRD patterns of 31 samples fabricated by L-DED in the Mo-Ta-Nb-W alloy system. This figure is quoted with permission from Moorehead *et al.*[194]; (D) XRD patterns of $CoCrFeNiNb_x$ printed in the authors' lab.

phase shows thinner magnetic stripe domains than the FCC phase, which leads to lower eddy losses as the BCC phase fraction increases.

Zhang *et al.* studied the effect of composition and phase fraction in a FeCoNi(CuAl)x alloy system on the magnetic and mechanical properties[201]. The general trend from Figure 17B shows that the saturation magnetization (M_s) decreases with increasing Cu and Al content and shows a slight increase from x = 0.8 to x = 0.9. Fe, Co, and Ni are all ferromagnetic elements, while Cu and Al are not, so the authors rationalize the decrease in M_s originating from the increase in non-ferromagnetic components. Borkar *et al.* also studied the effect of the Co/Cr ratio on the microstructure and magnetic properties of $AlCo_xCr_{1-x}FeNi$[202]. Increasing the Co/Cr ratio leads to increased M_s as the magnetization depends heavily on the composition, as shown in Figure 17C.

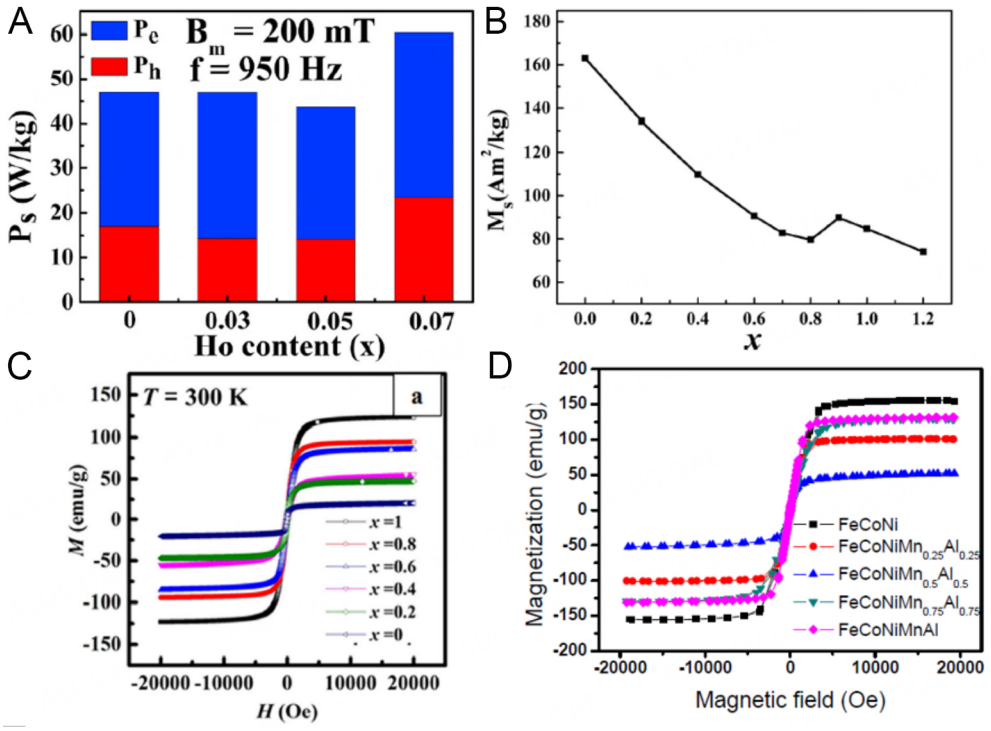

Figure 17. (A) Effect of Ho addition to $FeCoNi(CuAl)_{0.8}$ on magnetic hysteresis response of this alloy measured at room temperature. This figure is quoted with permission from Tang *et al.*[200], copyright 2021, Elsevier; (B) saturation magnetization of $FeCoNi(CuAl)_x$ alloys as CuAl is added. This figure is quoted with permission from Zhang *et al.*[201], copyright 2017, Elsevier; (C) magnetization curves of $NiAlFeCo_xCr_{1-x}$. This figure is quoted with permission from Borkar *et al.*[202], copyright 2017, John Wiley and Sons; (D) magnetization curves of $FeCoNi(MnAl)_x$. This figure is quoted with permission from Li *et al.*[203], copyright 2017, Elsevier.

Li *et al.* adjusted the composition of a $FeCoNi(MnAl)_x$ to study the effect of composition on the magnetic properties of this material[203]. The results presented in Figure 17D show that the saturation magnetization decreases as the Cu and Al content increases to x = 0.5 and then increases as the Cu, and Al content increases further. The FeCoNi alloy shows a fully FCC structure, while the $FeCoNi(MnAl)_{0.5}$ and $FeCoNi(MnAl)_{0.75}$ show an FCC + BCC dual-phase structure, and the FeCoNi(MnAl) composition shows a nearly fully BCC structure. Also, the lattice parameter of the FCC phase increases as Mn and Al are added, and the lattice parameter of the BCC phase decreases. The authors explain that the magnetization of the BCC phase decreases with decreasing lattice parameters and the magnetization of the FCC phase decreases with increasing lattice parameters[203]. Thus, the $FeCoNi(MnAl)_{0.5}$ composition shows the lowest magnetic performance because both phases show their lowest performance at that composition.

Corrosion resistance

Corrosion resistance is a crucial property when selecting materials for real-life applications. The degradation of materials due to corrosion leads to over $500 billion in repair and maintenance costs in the US alone[204]. The corrosion process is highly complicated and includes various mechanisms that depend on the type and concentration of the corrosive electrolyte, the composition and microstructure of the chosen material, the ambient temperature, and the time spent in service[185]. Due to the complexity of corrosion phenomena, there is currently no unifying computational model to predict corrosion resistance, and there are limited empirical models for certain systems. This challenge forces researchers to rely on experimental results to screen materials for corrosion resistance. Thus, high-throughput corrosion resistance methods are extremely important to characterize and screen HEAs for future applications. Typical high-throughput screening methods utilize multi-electrode arrays placed in a common electrolyte to allow multiple materials

to be tested simultaneously[205,206]. Rapid characterization via wire resistance to indicate a reduction in the cross-sectional area has shown great potential to accelerate the analysis of corrosion resistance[207]. Additionally, optical characterization of the color change of a corroded substance can be correlated well with traditional polarization curves. It can thus provide an easy screening method without the need for in-depth analysis[208,209]. The remainder of this section will summarize the results of combinatorial studies on HEAs taken from the literature that illustrate the improvements in corrosion resistance achieved so far.

It is well known that Cr is a useful element to improve corrosion resistance, and this result has also been verified for many HEA systems[210]. Thus, a Cr-containing HEA system with elements that show a low thermal neutron absorption cross-section is a prime candidate for nuclear applications[210]. Xiang *et al.* studied the effect of Cr addition in a $Mo_{0.5}$VNbTi system on the microstructure and properties, including corrosion resistance[210]. The corrosion resistance tests for the $Mo_{0.5}VNbTiCr_x$ HEAs (x = 0, 0.25, 0.5, 0.75, 1.0, 1.5, and 2.0, denoted as Cr_0, $Cr_{0.25}$, $Cr_{0.5}$, $Cr_{0.75}$, $Cr_{1.0}$, $Cr_{1.5}$, and $Cr_{2.0}$, respectively) was carried out in superheated steam at 400 °C at 10.3 MPa in a static autoclave which is in accordance with ASTM G2/G2M guidelines. The weight gain per unit surface area was measured after 10, 20, 30, 40, 50, 60, and 70 days. The weight gain for each sample was compared to that of Zr-4 alloy (Zr-1.41Sn-0.21Fe-0.10Cr), which is commonly used as fuel rod cladding in nuclear reactors due to its excellent corrosion resistance[210,211]. The results are depicted in Figure 18A, where the weight gain decreases with adding Cr, except for the $Cr_{1.5}$ alloy, which may be due to defects. All the compositions outperform the Zr-4 alloy showing much lower weight gain. This HEA system shows significantly improved corrosion resistance compared to a state-of-the-art alloy used in current applications, illustrating the potential of HEAs to achieve incredible improvements in corrosion resistance properties.

Q235 steel is a common structural steel used in many applications, but it often requires a coating to be used in corrosive environments[212]. A HEA coating with good corrosion resistance can offer protection to the Q235 steel without degradation to its mechanical properties[212]. Qiu *et al.* explored the effect of composition on corrosion resistance in the $Al_2CrFeCo_xCuNiTi$[212]. The addition of Co to the system leads to a more positive corrosion potential which implies a higher corrosion resistance especially compared to the control Q235 steel, as seen in Figure 18B. The authors mention that severe elemental segregation can lead to the formation of micro-potentials during potentiodynamic polarization tests which can lead to micro-corrosion and accelerate the corrosion process. The authors also note that the equiaxed grain structure observed in the HEAs also leads to improved corrosion resistance. Qiu *et al.* also conducted a similar study on $Al_2CrFeCoCuNi_xTi$[213]. Their results are illustrated in Figure 18C. It was also found that the corrosion resistance increased with increasing Ni content and then decreased. The increase in corrosion resistance is because the Ni element has a high corrosion resistance which contributes to the improved corrosion resistance of the alloy. However, as the Ni content increases further beyond $Ni_{1.0}$, the elemental segregation increases greatly, which leads to the formation of micro-potentials that accelerate the corrosion process.

Ti-Zr-based HEAs have been suggested as potential biomedical implant materials[214]. These implants invariably undergo friction wear over long periods, and the complex chemical environment of the human body also leads to corrosion. Thus, a comprehensive understanding of the corrosion and wear resistance of such HEAs is needed to assess their viability for use as implants. Hua *et al.* studied the corrosion resistance of $Ti_xZrNbTaMo$ HEAs and compared it to Ti-6Al-4V, which has long been favored for biomedical applications[215]. The corrosion resistance on these alloys is depicted through the potentiodynamic polarization curves in Figure 18D. The $Ti_{0.5}ZrNbTaMo$ composition shows the highest corrosion resistance[214]. SEM image analysis of all the tested compositions showed that no pitting occurred after the potentiodynamic polarization tests, which points to the high corrosion resistance of these alloys. Further

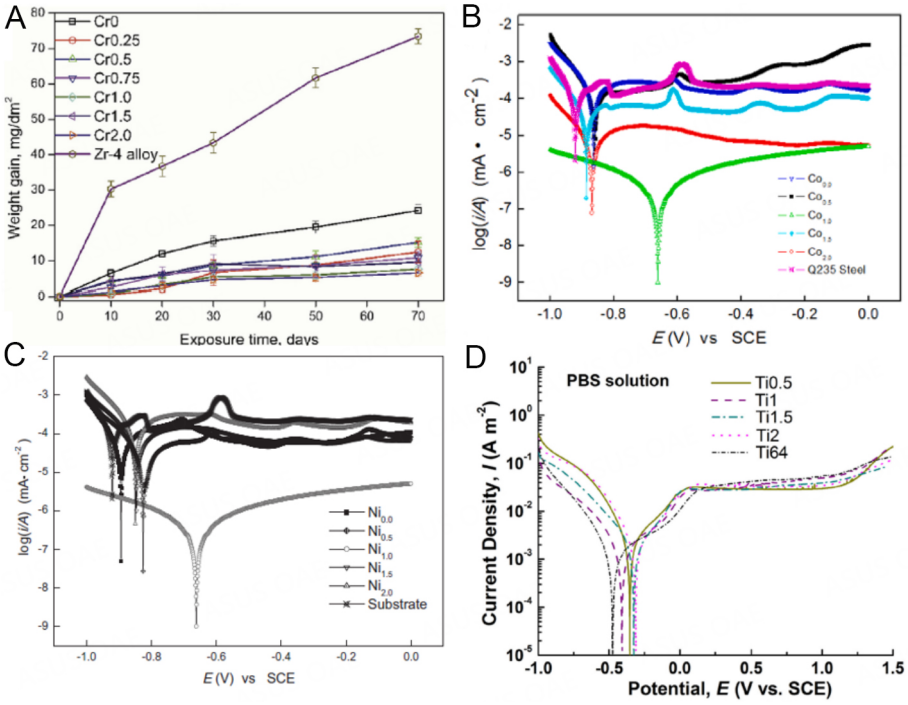

Figure 18. (A) Weight gain of $Mo_{0.5}VNbTiCr_x$ after corrosion test in superheated steam at 400 °C at 10.3 MPa pressure for 70 days, Zr-4 alloy is provided for comparison. This figure is quoted with permission from Xiang *et al.*[210], copyright 2020, Elsevier; (B) potentiodynamic polarization curves of $Al_2CrFeCo_xCuNiTi$ HEA compared to Q235 steel. This figure is quoted with permission from Qiu *et al.*[212], copyright 2019, Elsevier; (C) potentiodynamic polarization curves of $Al_2CrFeCoCuTiNi_x$ HEAs and Q235 steel substrate. This figure is quoted with permission from Qiu *et al.*[213], copyright 2013, Elsevier; (D) potentiodynamic polarization curves of $Ti_xZrNbTaMo$ HEAs and Ti6Al4V. This figure is quoted with permission from Hua *et al.*[214], copyright 2021, Elsevier.

surface analysis via XPS showed that the surface film of the HEAs is mainly composed of the Ti^{4+}, Zr^{4+}, Nb^{5+}, Ta^{5+}, Mo^{4+}, and Mo^{6+} oxides, which indicates the formation of a passivation layer that protected the alloys from severe corrosion.

CONCLUSIONS AND FUTURE OUTLOOK

HEAs present abundant opportunities to search for new materials with properties and performance that can exceed traditional dilute alloys. While the potential for this new class of materials is promising, the vast composition and microstructure space is too large to explore efficiently via traditional metallurgical techniques based on trial-and-error approaches. This review article highlights important advances in combinatorial studies that either present high-throughput methods to rapidly filter out undesirable materials or provide insights into general rules of thumb to allow researchers to design high-performance materials more efficiently.

The ultimate goal is to ensure that researchers spend more time understanding how to design and manufacture high-performance HEAs for industrial applications and less time on repetitive sample preparation and characterization methods. Implementing efficient high-throughput methods can minimize the time spent studying sub-optimal alloy compositions, which maximizes the resources spent on improving the most promising alloys. First, this review explores the high-throughput computational techniques that can down-select the design space before experimental characterization is even attempted. Then, it presents works that use additive manufacturing as a solution to produce large combinatorial libraries of bulk sample materials at length scales comparable to those expected during service and

applications. Finally, high-throughput material characterization is highlighted for rapid understanding of the relationships between composition, microstructure, and material properties. This review article serves as a guideline for developing workflows that can efficiently discover new high-performance HEAs. To this end, several research frontiers in the field are put forward:

1. Machine learning (ML) techniques can provide predictions of massive design space, but there currently exists a shortage of robust training sets for HEA compositions. Further investment in high-throughput computational techniques that can produce these robust databases, such as CALPHAD, first-principles calculations, and molecular dynamics simulation, is needed. Once these databases are sufficiently established, ML techniques can provide highly reliable predictions of the phase constitution for unknown compositions. They can even predict bulk properties such as yield strength and density.

2. Additive manufacturing provides a means to rapidly produce bulk samples of varying compositions and microstructures. However, AM materials are prone to defects that can significantly deteriorate performance. Further studies, including in-situ characterization during 3D printing, are needed to better characterize the small-scale physics, in-situ alloying chemistry, and macroscale defect formation to reduce the work needed in preliminary optimization.

3. Data collection and analysis of material characterization techniques need to be further automated to enable high-throughput characterization of enormous materials libraries without significant time investments from researchers. Such techniques as phase, composition and microstructure characterization may need to be carried out in parallel to maximize the efficient use of equipment with overlapping functionalities, such as SEM with EBSD capabilities. Additionally, data processing automation is critically needed to rapidly characterize the vast number of compositions that are explored in high-throughput experiments.

DECLARATIONS

Acknowledgments

This work is based upon research conducted at the Center for High Energy X-ray Sciences (CHESS), which is supported by the National Science Foundation under award (DMR-1829070). The authors are grateful to Katharine Shanks at CHESS for her support in data acquisition and analysis at the ID3A beamline.

Authors' contributions

Writing: Mooraj S
Manuscript supervision and editing: Chen W

Availability of Data and Materials

Not applicable.

Financial support and sponsorship

Chen W acknowledges the support from National Science Foundation (DMR-2004429) and UMass Amherst Faculty Startup Fund.

Conflicts of interest

All authors declare that there are no conflicts of interest.

Ethical approval and consent to participate

Not applicable.

Consent for publication

Not applicable.

REFERENCES

1. Oh HS, Kim SJ, Odbadrakh K, et al. Engineering atomic-level complexity in high-entropy and complex concentrated alloys. *Nat Commun* 2019;10:2090. DOI PubMed PMC
2. Cantor B. Multicomponent and high entropy alloys. *Entropy* 2014;16:4749. DOI
3. Cantor B, Chang I, Knight P, Vincent A. Microstructural development in equiatomic multicomponent alloys. *Mater Sci Eng A* 2004;375-377:213-8. DOI
4. Yeh J, Chen S, Lin S, et al. Nanostructured high-entropy alloys with multiple principal elements: novel alloy design concepts and outcomes. *Adv Eng Mater* 2004;6:299-303. DOI
5. George EP, Raabe D, Ritchie RO. High-entropy alloys. *Nat Rev Mater* 2019;4:515-34. DOI
6. Wu Q, Wang Z, Hu X, et al. Uncovering the eutectics design by machine learning in the Al-Co-Cr-Fe-Ni high entropy system. *Acta Mater* 2020;182:278-86. DOI
7. Chanda B, Verma A, Das J. Nano-/ultrafine eutectic in CoCrFeNi(Nb/Ta) high-entropy alloys. *Trans Indian Inst Met* 2018;71:2717-23. DOI
8. Zhang H, Liu P, Hou J, Qiao J, Wu Y. Prediction of strength and ductility in partially recrystallized $CoCrFeNiTi_{0.2}$ high-entropy alloy. *Entropy* 2019;21:389. DOI PubMed PMC
9. Zhou K, Li J, Wang L, Yang H, Wang Z, Wang J. Direct laser deposited bulk $CoCrFeNiNb_x$ high entropy alloys. *Intermetallics* 2019;114:106592. DOI
10. Poletti MG, Fiore G, Gili F, Mangherini D, Battezzati L. Development of a new high entropy alloy for wear resistance: $FeCoCrNiW_{0.3}$ and $FeCoCrNiW_{0.3}$ + 5 at.% of C. *Mater Design* 2017;115:247-54. DOI
11. Xiao J, Tan H, Chen J, Martini A, Zhang C. Effect of carbon content on microstructure, hardness and wear resistance of $CoCrFeMnNiC_x$ high-entropy alloys. *J Alloys Compd* 2020;847:156533. DOI
12. Cui Y, Shen J, Manladan SM, Geng K, Hu S. Wear resistance of $FeCoCrNiMnAl_x$ high-entropy alloy coatings at high temperature. *Appl Surf Sci* 2020;512:145736. DOI
13. Shi Y, Yang B, Liaw P. Corrosion-resistant high-entropy alloys: a review. *Metals* 2017;7:43. DOI
14. Li R, Xie L, Wang WY, Liaw PK, Zhang Y. High-throughput calculations for high-entropy alloys: a brief review. *Front Mater* 2020;7:290. DOI
15. Yin Y, Chen Z, Mo N, et al. High-temperature age-hardening of a novel cost-effective $Fe_{45}Ni_{25}Cr_{25}Mo_5$ high entropy alloy. *Mater Sci Eng A* 2020;788:139580. DOI
16. Ma Y, Wu S, Jia Y, et al. Hexagonal closed-packed precipitation enhancement in a NbTiHfZr refractory high-entropy alloy. *Metals* 2019;9:485. DOI
17. Liu Z, Zhao D, Wang P, et al. Additive manufacturing of metals: microstructure evolution and multistage control. *J Mater Sci Technol* 2022;100:224-36. DOI
18. Fu C, Li J, Bai J, et al. Effect of helium bubbles on irradiation hardening of additive manufacturing 316L stainless steel under high temperature He ions irradiation. *J Nucl Mater* 2021;550:152948. DOI
19. Farshidianfar MH, Khajepour A, Gerlich A. Real-time control of microstructure in laser additive manufacturing. *Int J Adv Manuf Technol* 2016;82:1173-86. DOI
20. Shamsaei N, Yadollahi A, Bian L, Thompson SM. An overview of Direct Laser Deposition for additive manufacturing; Part II: mechanical behavior, process parameter optimization and control. *Addit Manuf* 2015;8:12-35. DOI
21. Derimow N, Clark T, Abbaschian R. Solidification processing and cooling rate effects on hexagonal $Co_{22}Cr_{18}Cu_{20}Mn_{16}Ti_{24}$ high-entropy alloys. *Mater Chem Phys* 2020;240:122188. DOI
22. Xu X, Guo S, Nieh T, Liu C, Hirata A, Chen M. Effects of mixing enthalpy and cooling rate on phase formation of $Al_xCoCrCuFeNi$ high-entropy alloys. *Materialia* 2019;6:100292. DOI
23. Kube SA, Schroers J. Metastability in high entropy alloys. *Scr Mater* 2020;186:392-400. DOI
24. Braeckman B, Boydens F, Hidalgo H, et al. High entropy alloy thin films deposited by magnetron sputtering of powder targets. *Thin Solid Films* 2015;580:71-6. DOI
25. Al Hasan NM, Hou H, Sarkar S, et al. Combinatorial synthesis and high-throughput characterization of microstructure and phase transformation in Ni-Ti-Cu-V quaternary thin-film library. *Engineering* 2020;6:637-43. DOI
26. Liu X, Zou P, Song L, et al. Combinatorial high-throughput methods for designing hydrogen evolution reaction catalysts. *ACS Catal*

2022;12:3789-96. DOI

27. Ludwig A. Discovery of new materials using combinatorial synthesis and high-throughput characterization of thin-film materials libraries combined with computational methods. *NPJ Comput Mater* 2019;5:70. DOI
28. Shi Y, Yang B, Rack PD, Guo S, Liaw PK, Zhao Y. High-throughput synthesis and corrosion behavior of sputter-deposited nanocrystalline Al (CoCrFeNi)100- combinatorial high-entropy alloys. *Mater Design* 2020;195:109018. DOI
29. Kube SA, Sohn S, Uhl D, Datye A, Mehta A, Schroers J. Phase selection motifs in high entropy alloys revealed through combinatorial methods: large atomic size difference favors BCC over FCC. *Acta Mater* 2019;166:677-86. DOI
30. Keil T, Utt D, Bruder E, Stukowski A, Albe K, Durst K. Solid solution hardening in CrMnFeCoNi-based high entropy alloy systems studied by a combinatorial approach. *J Mater Res* 2021;36:2558-70. DOI
31. Geuser FD. High-throughput in-situ characterization and modeling of precipitation kinetics in compositionally graded alloys. *Acta Mater* 2015;101:1-9. DOI
32. Zhang X, Xiang Y. Combinatorial approaches for high-throughput characterization of mechanical properties. *J Materiomics* 2017;3:209-20. DOI
33. Wang Z, Zhang L, Li W, et al. A high-throughput approach to explore the multi-component alloy space: a case study of nickel-based superalloys. *J Alloys Compd* 2021;858:158100. DOI
34. Zhu C, Li C, Wu D, et al. A titanium alloys design method based on high-throughput experiments and machine learning. *J Mater Res Technol* 2021;11:2336-53. DOI
35. Liu YH, Fujita T, Aji DP, Matsuura M, Chen MW. Structural origins of Johari-Goldstein relaxation in a metallic glass. *Nat Commun* 2014;5:3238. DOI PubMed
36. Li MX, Zhao SF, Lu Z, et al. High-temperature bulk metallic glasses developed by combinatorial methods. *Nature* 2019;569:99-103. DOI PubMed
37. Frazier WE. Metal additive manufacturing: a review. *J Materi Eng Perform* 2014;23:1917-28. DOI
38. Ngo TD, Kashani A, Imbalzano G, Nguyen KT, Hui D. Additive manufacturing (3D printing): a review of materials, methods, applications and challenges. *Compos B Eng* 2018;143:172-96. DOI
39. Snow Z, Nassar AR, Reutzel EW. Invited review article: review of the formation and impact of flaws in powder bed fusion additive manufacturing. *Addit Manuf* 2020;36:101457. DOI
40. Clare A, Mishra R, Merklein M, et al. Alloy design and adaptation for additive manufacture. *J Mater Process Technol* 2022;299:117358. DOI
41. Bandyopadhyay A, Traxel KD. Invited review article: metal-additive manufacturing - Modeling strategies for application-optimized designs. *Addit Manuf* 2018;22:758-74. DOI PubMed PMC
42. Zhang C, Ouyang D, Pauly S, Liu L. 3D printing of bulk metallic glasses. *Mater Sci Eng R Rep* 2021;145:100625. DOI
43. Silva LJ, Souza DM, de Araújo DB, Reis RP, Scotti A. Concept and validation of an active cooling technique to mitigate heat accumulation in WAAM. *Int J Adv Manuf Technol* 2020;107:2513-23. DOI
44. Dhinakaran V, Ajith J, Fathima Yasin Fahmidha A, Jagadeesha T, Sathish T, Stalin B. Wire arc additive manufacturing (WAAM) process of nickel based superalloys - a review. *Mater Today* 2020;21:920-5. DOI
45. Kozamernik N, Bračun D, Klobčar D. WAAM system with interpass temperature control and forced cooling for near-net-shape printing of small metal components. *Int J Adv Manuf Technol* 2020;110:1955-68. DOI
46. Hou P, Mooraj S, Champagne VK, et al. Effect of build height on temperature evolution and thermally induced residual stresses in plasma arc additively manufactured stainless steel. *Metall Mater Trans A* 2022;53:627-39. DOI
47. Borkar T, Gwalani B, Choudhuri D, et al. A combinatorial assessment of $Al_xCrCuFeNi_2$ ($0 < x < 1.5$) complex concentrated alloys: microstructure, microhardness, and magnetic properties. *Acta Mater* 2016;116:63-76. DOI
48. Miracle D, Senkov O. A critical review of high entropy alloys and related concepts. *Acta Mater* 2017;122:448-511. DOI
49. Li Z, Raabe D. Strong and ductile non-equiatomic high-entropy alloys: design, processing, microstructure, and mechanical properties. *JOM* 2017;69:2099-106. DOI PubMed PMC
50. Choi W, Jung S, Jo YH, Lee S, Lee B. Design of new face-centered cubic high entropy alloys by thermodynamic calculation. *Met Mater Int* 2017;23:839-47. DOI
51. Yeh JW. Recent progress in high-entropy alloys. Available from: https://www.researchgate.net/profile/Jien-Wei-Yeh/publication/245440481_Recent_progress_in_high-entropy_alloys/links/02e7e52456c6fbaec9000000/Recent-progress-in-high-entropy-alloys.pdf [Last accessed on 16 Mar 2023].
52. Li H, Lai J, Li Z, Wang L. Multi-sites electrocatalysis in high-entropy alloys. *Adv Funct Mater* 2021;31:2106715. DOI
53. Marshal A, Pradeep K, Music D, Zaefferer S, De P, Schneider J. Combinatorial synthesis of high entropy alloys: introduction of a novel, single phase, body-centered-cubic FeMnCoCrAl solid solution. *J Alloys Compd* 2017;691:683-9. DOI
54. Yao H, Qiao J, Hawk J, Zhou H, Chen M, Gao M. Mechanical properties of refractory high-entropy alloys: experiments and modeling. *J Alloys Compd* 2017;696:1139-50. DOI
55. Zhang Y, Zhou Y, Lin J, Chen G, Liaw P. Solid-solution phase formation rules for multi-component alloys. *Adv Eng Mater* 2008;10:534-8. DOI
56. Bao N, Zuo J, Du Z, Yang M, Jiang G, Zhang L. Computational characterization of the structural and mechanical properties of Al_x $CoCrFeNiTi_{1-x}$ high entropy alloys. *Mater Res Express* 2019;6:096519. DOI
57. Dong Y, Chen QS, Lu YP, Zhang PC, Li TJ. Effect of aging temperature on microstructure and hardness of $CoCrFeNiTi_{0.5}$ high

entropy alloy. *Mater Sci Forum* 2014;789:48-53. DOI
58. Guo S, Ng C, Liu C. Anomalous solidification microstructures in Co-free $Al_xCrCuFeNi_2$ high-entropy alloys. *J Alloys Compd* 2013;557:77-81. DOI
59. Chen J, Zhou X, Wang W, et al. A review on fundamental of high entropy alloys with promising high-temperature properties. *J Alloys Compd* 2018;760:15-30. DOI
60. Stepanov N, Shaysultanov D, Ozerov M, Zherebtsov S, Salishchev G. Second phase formation in the CoCrFeNiMn high entropy alloy after recrystallization annealing. *Mater Lett* 2016;185:1-4. DOI
61. Toda-caraballo I, Rivera-díaz-del-castillo PE. Modelling solid solution hardening in high entropy alloys. *Acta Mater* 2015;85:14-23. DOI
62. He Q, Yang Y. On lattice distortion in high entropy alloys. *Front Mater* 2018;5:42. DOI
63. Lee C, Chou Y, Kim G, et al. Lattice-distortion-enhanced yield strength in a refractory high-entropy alloy. *Adv Mater* 2020;32:e2004029. DOI PubMed
64. Lee C, Song G, Gao MC, et al. Lattice distortion in a strong and ductile refractory high-entropy alloy. *Acta Mater* 2018;160:158-72. DOI
65. Dirras G, Lilensten L, Djemia P, et al. Elastic and plastic properties of as-cast equimolar TiHfZrTaNb high-entropy alloy. *Mater Sci Eng A* 2016;654:30-8. DOI
66. Owen L, Pickering E, Playford H, Stone H, Tucker M, Jones N. An assessment of the lattice strain in the CrMnFeCoNi high-entropy alloy. *Acta Mater* 2017;122:11-8. DOI
67. Senkov O, Scott J, Senkova S, Miracle D, Woodward C. Microstructure and room temperature properties of a high-entropy TaNbHfZrTi alloy. *J Alloys Compd* 2011;509:6043-8. DOI
68. Guo S. Phase selection rules for cast high entropy alloys: an overview. *Mater Sci Technol* 2015;31:1223-30. DOI
69. Zhang Y, Lu ZP, Ma SG, et al. Guidelines in predicting phase formation of high-entropy alloys. *MRS Commun* 2014;4:57-62. DOI
70. Kottke J, Laurent-brocq M, Fareed A, et al. Tracer diffusion in the Ni-CoCrFeMn system: transition from a dilute solid solution to a high entropy alloy. *Scr Mater* 2019;159:94-8. DOI
71. Mehta A, Sohn Y. Investigation of sluggish diffusion in FCC $Al_{0.25}$CoCrFeNi high-entropy alloy. *Mate Res Lett* 2021;9:239-46. DOI
72. Dąbrowa J, Danielewski M. State-of-the-art diffusion studies in the high entropy alloys. *Metals* 2020;10:347. DOI
73. Sathiaraj G, Ahmed M, Bhattacharjee P. Microstructure and texture of heavily cold-rolled and annealed fcc equiatomic medium to high entropy alloys. *J Alloys Compd* 2016;664:109-19. DOI
74. Bhattacharjee P, Sathiaraj G, Zaid M, et al. Microstructure and texture evolution during annealing of equiatomic CoCrFeMnNi high-entropy alloy. *J Alloys Compd* 2014;587:544-52. DOI
75. Sathiaraj G, Bhattacharjee P. Effect of starting grain size on the evolution of microstructure and texture during thermo-mechanical processing of CoCrFeMnNi high entropy alloy. *J Alloys Compd* 2015;647:82-96. DOI
76. Ranganathan S. Alloyed pleasures: multimetallic cocktails. Available from: http://eprints.iisc.ac.in/6189/1/Alloyed_pleasures.pdf [Last accessed on 16 Mar 2023].
77. Qiao L, Liu Y, Zhu J. A focused review on machine learning aided high-throughput methods in high entropy alloy. *J Alloys Compd* 2021;877:160295. DOI
78. Butler KT, Davies DW, Cartwright H, Isayev O, Walsh A. Machine learning for molecular and materials science. *Nature* 2018;559:547-55. DOI PubMed
79. Yang C, Ren C, Jia Y, Wang G, Li M, Lu W. A machine learning-based alloy design system to facilitate the rational design of high entropy alloys with enhanced hardness. *Acta Mater* 2022;222:117431. DOI
80. Krishna YV, Jaiswal UK, Rahul RM. Machine learning approach to predict new multiphase high entropy alloys. *Scr Mater* 2021;197:113804. DOI
81. Zhou T, Song Z, Sundmacher K. Big data creates new opportunities for materials research: a review on methods and applications of machine learning for materials design. *Engineering* 2019;5:1017-26. DOI
82. Liu X, Xu P, Zhao J, Lu W, Li M, Wang G. Material machine learning for alloys: Applications, challenges and perspectives. *J Alloys Compd* 2022;921:165984. DOI
83. Liu S, Kappes BB, Amin-ahmadi B, Benafan O, Zhang X, Stebner AP. Physics-informed machine learning for composition - process - property design: shape memory alloy demonstration. *Appl Mater Today* 2021;22:100898. DOI
84. Yi W, Liu G, Lu Z, Gao J, Zhang L. Efficient alloy design of Sr-modified A356 alloys driven by computational thermodynamics and machine learning. *J Mater Sci Technol* 2022;112:277-90. DOI
85. White AD. Deep learning for molecules and materials. *LiveCoMS* 2022:3. DOI
86. Nassar A, Mullis A. Rapid screening of high-entropy alloys using neural networks and constituent elements. *Comput Mater Sci* 2021;199:110755. DOI
87. Risal S, Zhu W, Guillen P, Sun L. Improving phase prediction accuracy for high entropy alloys with machine learning. *Comput Mater Sci* 2021;192:110389. DOI
88. Montavon G, Samek W, Müller K. Methods for interpreting and understanding deep neural networks. *Digit Signal Process* 2018;73:1-15. DOI
89. Zhang Y, Wen C, Wang C, et al. Phase prediction in high entropy alloys with a rational selection of materials descriptors and machine learning models. *Acta Mater* 2020;185:528-39. DOI

90. Vazquez G, Singh P, Sauceda D, et al. Efficient machine-learning model for fast assessment of elastic properties of high-entropy alloys. *Acta Mater* 2022;232:117924. DOI
91. Purcell TAR, Scheffler M, Carbogno C, Ghiringhelli LM. SISSO++: A C++ implementation of the sure-independence screening and sparsifying operator approach. *J Open Res Softw* 2022;7:3960. DOI
92. Sorkin V, Yu ZG, Chen S, Tan TL, Aitken ZH, Zhang YW. A first-principles-based high fidelity, high throughput approach for the design of high entropy alloys. *Sci Rep* 2022;12:11894. DOI PubMed PMC
93. Hautier G, Jain A, Ong SP. From the computer to the laboratory: materials discovery and design using first-principles calculations. *J Mater Sci* 2012;47:7317-40. DOI
94. Ikeda Y, Grabowski B, Körmann F. Ab initio phase stabilities and mechanical properties of multicomponent alloys: a comprehensive review for high entropy alloys and compositionally complex alloys. *Mater Charact* 2019;147:464-511. DOI
95. Kohn W, Sham LJ. Self-consistent equations including exchange and correlation effects. *Phys Rev* 1965;140:A1133-8. DOI
96. Ceperley DM, Alder BJ. Ground state of the electron gas by a stochastic method. *Phys Rev Lett* 1980;45:566-9. DOI
97. Perdew JP. Density-functional approximation for the correlation energy of the inhomogeneous electron gas. *Phys Rev B Condens Matter* 1986;33:8822-4. DOI
98. Perdew JP, Burke K, Ernzerhof M. Generalized gradient approximation made simple. *Phys Rev Lett* 1996;77:3865-8. DOI PubMed
99. Perdew JP, Chevary JA, Vosko SH, et al. Atoms, molecules, solids, and surfaces: applications of the generalized gradient approximation for exchange and correlation. *Phys Rev B Condens Matter* 1992;46:6671-87. DOI
100. Kim G, Diao H, Lee C, et al. First-principles and machine learning predictions of elasticity in severely lattice-distorted high-entropy alloys with experimental validation. *Acta Mater* 2019;181:124-38. DOI
101. Rittiruam M, Noppakhun J, Setasuban S, et al. High-throughput materials screening algorithm based on first-principles density functional theory and artificial neural network for high-entropy alloys. *Sci Rep* 2022;12:16653. DOI PubMed PMC
102. Bellaiche L, Vanderbilt D. Virtual crystal approximation revisited: application to dielectric and piezoelectric properties of perovskites. *Phys Rev B* 2000;61:7877-82. DOI
103. Ramer N, Rappe A. Application of a new virtual crystal approach for the study of disordered perovskites. *J Phys Chem Solids* 2000;61:315-20. DOI
104. Chen L, Hao X, Wang Y, Zhang X, Liu H. First-principles calculation of the effect of Ti content on the structure and properties of TiVNbMo refractory high-entropy alloy. *Mater Res Express* 2020;7:106516. DOI
105. Lederer Y, Toher C, Vecchio KS, Curtarolo S. The search for high entropy alloys: a high-throughput ab-initio approach. *Acta Mater* 2018;159:364-83. DOI
106. Curtarolo S, Setyawan W, Hart GL, et al. AFLOW: an automatic framework for high-throughput materials discovery. *Comput Mater Sci* 2012;58:218-26. DOI
107. Sanchez J, Ducastelle F, Gratias D. Generalized cluster description of multicomponent systems. *Physica A* 1984;128:334-50. DOI
108. de Walle A, Asta M, Ceder G. The alloy theoretic automated toolkit: a user guide. *Calphad* 2002;26:539-53. DOI
109. Berding MA, Sher A. Electronic quasichemical formalism: application to arsenic deactivation in silicon. *Phys Rev B* 1998;58:3853-64. DOI
110. Jiang L, Lu Y, Jiang H, et al. Formation rules of single phase solid solution in high entropy alloys. *Mater Sci Technol* 2015. DOI
111. Guo S, Ng C, Lu J, Liu CT. Effect of valence electron concentration on stability of fcc or bcc phase in high entropy alloys. *J Appl Phys* 2011;109:103505. DOI
112. Yang S, Liu G, Zhong Y. Revisit the VEC criterion in high entropy alloys (HEAs) with high-throughput ab initio calculations: a case study with Al-Co-Cr-Fe-Ni system. *J Alloys Compd* 2022;916:165477. DOI
113. Zhou K & Liu B. Molecular dynamics simulation: fundamentals and applications. Academic Press; 2022. DOI
114. Car R, de Angelis F, Giannozzi P, Marzari N. First-principles molecular dynamics. In: Yip S, editor. Handbook of Materials Modeling. Dordrecht: Springer; 2005. pp. 59-76. DOI
115. Tang Y, Li D. Nano-tribological behavior of high-entropy alloys CrMnFeCoNi and CrFeCoNi under different conditions: a molecular dynamics study. *Wear* 2021;476:203583. DOI
116. Yin S, Zuo Y, Abu-Odeh A, et al. Atomistic simulations of dislocation mobility in refractory high-entropy alloys and the effect of chemical short-range order. *Nat Commun* 2021;12:4873. DOI PubMed PMC
117. Fan Y, Wang W, Hao Z, Zhan C. Work hardening mechanism based on molecular dynamics simulation in cutting Ni-Fe-Cr series of Ni-based alloy. *J Alloys Compd* 2020;819:153331. DOI
118. Li J, Fang Q, Liu B, Liu Y, Liu Y. Mechanical behaviors of AlCrFeCuNi high-entropy alloys under uniaxial tension via molecular dynamics simulation. *RSC Adv* 2016;6:76409-19. DOI
119. Trong DN, Long VC, Ţălu Ş. Effects of number of atoms and doping concentration on the structure, phase transition, and crystallization process of $Fe_{1-x-y}Ni_xCo_y$ alloy: a molecular dynamic study. *Appl Sci* 2022;12:8473. DOI
120. Xie L, Brault P, Thomann A, Yang X, Zhang Y, Shang G. Molecular dynamics simulation of Al-Co-Cr-Cu-Fe-Ni high entropy alloy thin film growth. *Intermetallics* 2016;68:78-86. DOI
121. Pan Z, Fu Y, Wei Y, Yan X, Luo H, Li X. Deformation mechanisms of TRIP-TWIP medium-entropy alloys via molecular dynamics simulations. *Int J Mech Sci* 2022;219:107098. DOI
122. Jarlöv A, Ji W, Zhu Z, et al. Molecular dynamics study on the strengthening mechanisms of Cr-Fe-Co-Ni high-entropy alloys based on the generalized stacking fault energy. *J Alloys Compd* 2022;905:164137. DOI

123. Li J, Xie B, Fang Q, Liu B, Liu Y, Liaw PK. High-throughput simulation combined machine learning search for optimum elemental composition in medium entropy alloy. *J Mater Sci Technol* 2021;68:70-5. DOI
124. Zhang L, Qian K, Huang J, Liu M, Shibuta Y. Molecular dynamics simulation and machine learning of mechanical response in non-equiatomic FeCrNiCoMn high-entropy alloy. *J Mater Res Technol* 2021;13:2043-54. DOI
125. Morrissey LS, Nakhla S. Considerations when calculating the mechanical properties of single crystals and bulk polycrystals from molecular dynamics simulations. *Mol Simul* 2020;46:1433-42. DOI
126. Zhang L, Qian K, Schuller BW, Shibuta Y. Prediction on mechanical properties of non-equiatomic high-entropy alloy by atomistic simulation and machine learning. *Metals* 2021;11:922. DOI
127. Jiang J, Sun W, Luo N. Molecular dynamics study of microscopic deformation mechanism and tensile properties in Al_xCoCrFeNi amorphous high-entropy alloys. *Mater Today Commun* 2022;31:103861. DOI
128. Guruvidyathri K, Hari Kumar KC, Yeh JW, Murty BS. Topologically close-packed phase formation in high entropy alloys: a review of calphad and experimental results. *JOM* 2017;69:2113-24. DOI
129. Gao MC. Design of high-entropy alloys. In: Gao MC, Yeh J, Liaw PK, Zhang Y, editors. High-entropy alloys. Cham: Springer International Publishing; 2016. pp. 369-98. DOI
130. Senkov ON, Miller JD, Miracle DB, Woodward C. Accelerated exploration of multi-principal element alloys with solid solution phases. *Nat Commun* 2015;6:6529. DOI PubMed PMC
131. Klaver TPC, Simonovic D, Sluiter MHF. Brute force composition scanning with a CALPHAD database to find low temperature body centered cubic high entropy alloys. *Entropy* 2018;20:911. DOI PubMed PMC
132. Thurston KV, Gludovatz B, Hohenwarter A, Laplanche G, George EP, Ritchie RO. Effect of temperature on the fatigue-crack growth behavior of the high-entropy alloy CrMnFeCoNi. *Intermetallics* 2017;88:65-72. DOI
133. Li YJ, Savan A, Ludwig A. Atomic scale understanding of phase stability and decomposition of a nanocrystalline CrMnFeCoNi Cantor alloy. *Appl Phys Lett* 2021;119:201910. DOI
134. Zeng Z, Xiang M, Zhang D, et al. Mechanical properties of Cantor alloys driven by additional elements: a review. *J Mater Res Technol* 2021;15:1920-34. DOI
135. Conway PL, Klaver T, Steggo J, Ghassemali E. High entropy alloys towards industrial applications: high-throughput screening and experimental investigation. *Mater Sci Eng A* 2022;830:142297. DOI
136. Abu-odeh A, Galvan E, Kirk T, et al. Efficient exploration of the high entropy alloy composition-phase space. *Acta Mater* 2018;152:41-57. DOI
137. Zhao DQ, Pan SP, Zhang Y, Liaw PK, Qiao JW. Structure prediction in high-entropy alloys with machine learning. *Appl Phys Lett* 2021;118:231904. DOI
138. Schleder GR, Padilha ACM, Acosta CM, Costa M, Fazzio A. From DFT to machine learning: recent approaches to materials science-a review. *J Phys Mater* 2019;2:032001. DOI
139. Zhou Z, Zhou Y, He Q, Ding Z, Li F, Yang Y. Machine learning guided appraisal and exploration of phase design for high entropy alloys. *NPJ Comput Mater* 2019:5. DOI
140. Davydov AV, Kattner UR. Predicting synthesizability. *J Phys D Appl Phys* 2019;52:013001. DOI PubMed PMC
141. Jiang J, Chen P, Qiu J, et al. Microstructural evolution and mechanical properties of Al_xCoCrFeNi high-entropy alloys under uniaxial tension: a molecular dynamics simulations study. *Mater Today Commun* 2021;28:102525. DOI
142. Wang L, Liu W, Zhu B, et al. Influences of strain rate, Al concentration and grain heterogeneity on mechanical behavior of $CoNiFeAl_xCu_{1-x}$ high-entropy alloys: a molecular dynamics simulation. *J Mater Res Technol* 2021;14:2071-84. DOI
143. Leong Z, Tan TL. Robust cluster expansion of multicomponent systems using structured sparsity. *Phys Rev B* 2019:100. DOI
144. Leong Z, Ramamurty U, Tan TL. Microstructural and compositional design principles for Mo-V-Nb-Ti-Zr multi-principal element alloys: a high-throughput first-principles study. *Acta Mater* 2021;213:116958. DOI
145. Fernández-caballero A, Wróbel JS, Mummery PM, Nguyen-manh D. Short-range order in high entropy alloys: theoretical formulation and application to Mo-Nb-Ta-V-W system. *J Phase Equilib Diffus* 2017;38:391-403. DOI
146. Fontaine D. The number of independent pair-correlation functions in multicomponent systems. *J Appl Crystallogr* 1971;4:15-9. DOI
147. Kattner UR. The calphad method and its role in material and process development. *Tecnol Metal Mater Min* 2016;13:3-15. DOI PubMed PMC
148. Zeng Y, Man M, Bai K, Zhang Y. Revealing high-fidelity phase selection rules for high entropy alloys: a combined CALPHAD and machine learning study. *Mater Design* 2021;202:109532. DOI
149. Wu D, Tian Y, Zhang L, et al. Optimal design of high-strength Ti-Al-V-Zr alloys through a combinatorial approach. *Materials* 2018;11:1603. DOI PubMed PMC
150. Gumbmann E, De Geuser F, Deschamps A, Lefebvre W, Robaut F, Sigli C. A combinatorial approach for studying the effect of Mg concentration on precipitation in an Al-Cu-Li alloy. *Scr Mater* 2016;110:44-7. DOI
151. Li Y, Jensen KE, Liu Y, et al. Combinatorial strategies for synthesis and characterization of alloy microstructures over large compositional ranges. *ACS Comb Sci* 2016;18:630-7. DOI PubMed
152. Tang M, Pistorius PC, Narra S, Beuth JL. Rapid solidification: selective laser melting of $AlSi_{10}Mg$. *JOM* 2016;68:960-6. DOI
153. Aboutaleb AM, Mahtabi MJ, Tschopp MA, Bian L. Multi-objective accelerated process optimization of mechanical properties in laser-based additive manufacturing: case study on Selective Laser Melting (SLM) Ti-6Al-4V. *J Manuf Process* 2019;38:432-44. DOI
154. Jung HY, Peter NJ, Gärtner E, Dehm G, Uhlenwinkel V, Jägle EA. Bulk nanostructured AlCoCrFeMnNi chemically complex alloy

synthesized by laser-powder bed fusion. *Addit Manuf* 2020;35:101337. DOI

155. Lu Y, Su S, Zhang S, et al. Controllable additive manufacturing of gradient bulk metallic glass composite with high strength and tensile ductility. *Acta Mater* 2021;206:116632. DOI
156. Ren J, Zhang Y, Zhao D, et al. Strong yet ductile nanolamellar high-entropy alloys by additive manufacturing. *Nature* 2022;608:62-8. DOI PubMed
157. Zhang S, Hou P, Mooraj S, Chen W. Printability of $Zr_{41.2}Ti_{13.8}Cu_{12.5}Ni_{10.0}Be_{22.5}$ metallic glass on steel by laser additive manufacturing: a single-track study. *Surf Coat Technol* 2021;428:127882. DOI
158. Wang YM, Voisin T, McKeown JT, et al. Additively manufactured hierarchical stainless steels with high strength and ductility. *Nat Mater* 2018;17:63-71. DOI PubMed
159. Chen W, Voisin T, Zhang Y, et al. Microscale residual stresses in additively manufactured stainless steel. *Nat Commun* 2019;10:4338. DOI
160. Li Z, Ludwig A, Savan A, Springer H, Raabe D. Combinatorial metallurgical synthesis and processing of high-entropy alloys. *J Mater Res* 2018;33:3156-69. DOI
161. Santa-aho S, Kiviluoma M, Jokiaho T, et al. Additive manufactured 316L stainless-steel samples: microstructure, residual stress and corrosion characteristics after post-processing. *Metals* 2021;11:182. DOI
162. Zhang C, Chen F, Huang Z, et al. Additive manufacturing of functionally graded materials: a review. *Mater Sci Eng A* 2019;764:138209. DOI
163. del Val J, Arias-gonzález F, Barro O, et al. Functionally graded 3D structures produced by laser cladding. *Procedia Manuf* 2017;13:169-76. DOI
164. Gwalani B, Gangireddy S, Shukla S, et al. Compositionally graded high entropy alloy with a strong front and ductile back. *Mater Today Commun* 2019;20:100602. DOI
165. Li L, Wang J, Lin P, Liu H. Microstructure and mechanical properties of functionally graded TiC_p/Ti6Al4V composite fabricated by laser melting deposition. *Ceram Int* 2017;43:16638-51. DOI
166. Pegues JW, Melia MA, Puckett R, Whetten SR, Argibay N, Kustas AB. Exploring additive manufacturing as a high-throughput screening tool for multiphase high entropy alloys. *Addit Manuf* 2021;37:101598. DOI
167. Wen Y, Zhang B, Narayan RL, et al. Laser powder bed fusion of compositionally graded CoCrMo-Inconel 718. *Addit Manuf* 2021;40:101926. DOI
168. Shishkovsky I, Kakovkina N, Scherbakov V. Rapid TMC laser prototyping: Compositional and phase-structural sustainability via combinatorial design of titanium-based gradient alloy reinforced by nano-sized TiC or TiB_2 ceramics. *SPIE* 2018;10523:172-7. DOI
169. Traxel KD, Bandyopadhyay A. Influence of in situ ceramic reinforcement towards tailoring titanium matrix composites using laser-based additive manufacturing. *Addit Manuf* 2020;31:101004. DOI PubMed PMC
170. Gong X, Yabansu YC, Collins PC, Kalidindi SR. Evaluation of Ti-Mn alloys for additive manufacturing using high-throughput experimental assays and gaussian process regression. *Materials* 2020;13:4641. DOI PubMed PMC
171. Li M, Flores KM. Laser processing as a high-throughput method to investigate microstructure-processing-property relationships in multiprincipal element alloys. *J Alloys Compd* 2020;825:154025. DOI
172. Teh WH, Chaudhary V, Chen S, et al. High throughput multi-property evaluation of additively manufactured Co-Fe-Ni materials libraries. *Addit Manuf* 2022;58:102983. DOI
173. Gwalani B, Soni V, Waseem OA, Mantri SA, Banerjee R. Laser additive manufacturing of compositionally graded AlCrFeMoVx (x = 0 to 1) high-entropy alloy system. *Opt Laser Technol* 2019;113:330-7. DOI
174. Zhao Y, Lau KB, Teh WH, et al. Compositionally graded CoCrFeNiTi high-entropy alloys manufactured by laser powder bed fusion: a combinatorial assessment. *J Alloys Compd* 2021;883:160825. DOI
175. Yu Z, Zheng W, Li Z, et al. Accelerated exploration of TRIP metallic glass composite by laser additive manufacturing. *J Mater Sci Technol* 2021;78:68-73. DOI
176. Wu Y, Wang H, Liu X, et al. Designing bulk metallic glass composites with enhanced formability and plasticity. *J Mater Sci Technol* 2014;30:566-75. DOI
177. Zhai L, Lu Y, Zhao X, Wang L, Lu X. High-throughput screening of laser additive manufactured metallic glass via ultrasonic wave. *Sci Rep* 2019;9:17660. DOI PubMed PMC
178. Tsai P, Flores KM. High-throughput discovery and characterization of multicomponent bulk metallic glass alloys. *Acta Mater* 2016;120:426-34. DOI
179. Tsai P, Flores KM. A combinatorial strategy for metallic glass design via laser deposition. *Intermetallics* 2014;55:162-6. DOI
180. Islam Z, Nelaturu P, Thoma DJ. A dimensionless number for high-throughput design of multi-principal element alloys in directed energy deposition. *Appl Phys Lett* 2021;119:231901. DOI
181. Zhang W, Liu L, Peng S, et al. The tensile property and notch sensitivity of $AlCoCrFeNi_{2.1}$ high entropy alloy with a novel "steel-frame" eutectic microstructure. *J Alloys Compd* 2021;863:158747. DOI
182. Joseph J, Imran M, Hodgson P, Barnett M, Fabijanic D. Towards the large-scale production and strength prediction of near-eutectic $Al_xCoCrFeNi_{2.1}$ alloys by additive manufacturing. *Manuf Lett* 2020;25:16-20. DOI
183. Moorehead M, Nelaturu P, Elbakhshwan M, et al. High-throughput ion irradiation of additively manufactured compositionally complex alloys. *J Nucl Mater* 2021;547:152782. DOI
184. Miracle D, Majumdar B, Wertz K, Gorsse S. New strategies and tests to accelerate discovery and development of multi-principal

element structural alloys. *Scr Mater* 2017;127:195-200. DOI
185. Miracle DB, Li M, Zhang Z, Mishra R, Flores KM. Emerging capabilities for the high-throughput characterization of structural materials. *Annu Rev Mater Res* 2021;51:131-64. DOI
186. Pathak S, Kalidindi SR. Spherical nanoindentation stress-strain curves. *Mater Sci Eng R Rep* 2015;91:1-36. DOI
187. Jiang L, Cao Z, Jie J, et al. Effect of Mo and Ni elements on microstructure evolution and mechanical properties of the $CoFeNi_xVMo_y$ high entropy alloys. *J Alloys Compd* 2015;649:585-90. DOI
188. Ma S, Zhang Y. Effect of Nb addition on the microstructure and properties of AlCoCrFeNi high-entropy alloy. *Mater Sci Eng A* 2012;532:480-6. DOI
189. Wang X, Liu Q, Huang Y, Xie L, Xu Q, Zhao T. Effect of Ti content on the microstructure and corrosion resistance of $CoCrFeNiTi_x$ high entropy alloys prepared by laser cladding. *Materials* 2020;13:2209. DOI PubMed PMC
190. Shun T, Chang L, Shiu M. Microstructures and mechanical properties of multiprincipal component $CoCrFeNiTi_x$ alloys. *Mater Sci Eng A* 2012;556:170-4. DOI
191. Tong Y, Chen D, Han B, et al. Outstanding tensile properties of a precipitation-strengthened $FeCoNiCrTi_{0.2}$ high-entropy alloy at room and cryogenic temperatures. *Acta Mater* 2019;165:228-40. DOI
192. Huang K, Kain C, Diaz-vallejo N, Sohn Y, Zhou L. High throughput mechanical testing platform and application in metal additive manufacturing and process optimization. *J Manuf Process* 2021;66:494-505. DOI
193. Chen R, Qin G, Zheng H, et al. Composition design of high entropy alloys using the valence electron concentration to balance strength and ductility. *Acta Mater* 2018;144:129-37. DOI
194. Moorehead M, Bertsch K, Niezgoda M, et al. High-throughput synthesis of Mo-Nb-Ta-W high-entropy alloys via additive manufacturing. *Mater Design* 2020;187:108358. DOI
195. Ren F, Pandolfi R, Van Campen D, Hexemer A, Mehta A. On-the-fly data assessment for high-throughput X-ray diffraction measurements. *ACS Comb Sci* 2017;19:377-85. DOI PubMed
196. Long CJ, Bunker D, Li X, Karen VL, Takeuchi I. Rapid identification of structural phases in combinatorial thin-film libraries using X-ray diffraction and non-negative matrix factorization. *Rev Sci Instrum* 2009;80:103902. DOI PubMed
197. Datye A, Alexander Kube S, Verma D, Schroers J, Schwarz UD. Accelerated discovery and mechanical property characterization of bioresorbable amorphous alloys in the Mg-Zn-Ca and the Fe-Mg-Zn systems using high-throughput methods. *J Mater Chem B* 2019;7:5392-400. DOI PubMed
198. Zhao L, Jiang L, Yang L, et al. High throughput synthesis enabled exploration of CoCrFeNi-based high entropy alloys. *J Mater Sci Technol* 2022;110:269-82. DOI
199. Kaufmann K, Zhu C, Rosengarten AS, Maryanovsky D, Wang H, Vecchio KS. Phase mapping in EBSD using convolutional neural networks. *Microsc Microanal* 2020;26:458-68. DOI PubMed
200. Tang Y, Sun S, Lv M, et al. Effect of Ho addition on AC soft magnetic property, microstructure and magnetic domain of $FeCoNi(CuAl)_{0.8}Ho_x$ (x = 0-0.07) high-entropy alloys. *Intermetallics* 2021;135:107216. DOI
201. Zhang Q, Xu H, Tan X, et al. The effects of phase constitution on magnetic and mechanical properties of FeCoNi(CuAl) (x = 0-1.2) high-entropy alloys. *J Alloys Compd* 2017;693:1061-7. DOI
202. Borkar T, Chaudhary V, Gwalani B, et al. A combinatorial approach for assessing the magnetic properties of high entropy alloys: role of Cr in $AlCo_xCr_{1-x}FeNi$. *Adv Eng Mater* 2017;19:1700048. DOI
203. Li P, Wang A, Liu C. Composition dependence of structure, physical and mechanical properties of $FeCoNi(MnAl)_x$ high entropy alloys. *Intermetallics* 2017;87:21-6. DOI
204. Taylor CD, Lu P, Saal J, Frankel GS, Scully JR. Integrated computational materials engineering of corrosion resistant alloys. *NPJ Mater Degrad* 2018:2. DOI
205. Taylor SR. The investigation of corrosion phenomena with high throughput methods: a review. *Corros Rev* 2011;29:135-51. DOI
206. Muster T, Trinchi A, Markley T, et al. A review of high throughput and combinatorial electrochemistry. *Electrochim Acta* 2011;56:9679-99. DOI
207. Whitfield MJ, Bono D, Wei L, Van Vliet KJ. High-throughput corrosion quantification in varied microenvironments. *Corros Sci* 2014;88:481-6. DOI
208. White P, Smith G, Harvey T, et al. A new high-throughput method for corrosion testing. *Corros Sci* 2012;58:327-31. DOI
209. Liu J, Liu N, Sun M, Li J, Sohn S, Schroers J. Fast screening of corrosion trends in metallic glasses. *ACS Comb Sci* 2019;21:666-74. DOI PubMed
210. Xiang C, Fu H, Zhang Z, et al. Effect of Cr content on microstructure and properties of $Mo_{0.5}VNbTiCr_x$ high-entropy alloys. *J Alloys Compd* 2020;818:153352. DOI
211. Renčiuková V, Macák J, Sajdl P, Novotný R, Krausová A. Corrosion of zirconium alloys demonstrated by using impedance spectroscopy. *J Nucl Mater* 2018;510:312-21. DOI
212. Qiu X. Corrosion behavior of $Al_2CrFeCo_xCuNiTi$ high-entropy alloy coating in alkaline solution and salt solution. *Results Phys* 2019;12:1737-41. DOI
213. Qiu X, Liu C. Microstructure and properties of $Al_2CrFeCoCuTiNi_x$ high-entropy alloys prepared by laser cladding. *J Alloys Compd* 2013;553:216-20. DOI
214. Hua N, Wang W, Wang Q, et al. Mechanical, corrosion, and wear properties of biomedical Ti-Zr-Nb-Ta-Mo high entropy alloys. *J Alloys Compd* 2021;861:157997. DOI

215. Elias CN, Lima JHC, Valiev R, Meyers MA. Biomedical applications of titanium and its alloys. *JOM* 2008;60:46-9. DOI